Tunable Wettability of Microstructured Polypyrrole Films

by

Jean H. Chang

S.B., Massachusetts Institute of Technology (2008)

Submitted to the Department of Mechanical Engineering
in partial fulfillment of the requirements for the degree of

Master of Science in Mechanical Engineering

at the

MASSACHUSETTS INSTITUTE OF TECHNOLOGY

September 2010

Author .....
Department of Mechanical Engineering
August 5, 2010

Certified by .....
Ian W. Hunter
Hatsopoulos Professor of Mechanical Engineering
Thesis Supervisor

Accepted by .....
David E. Hardt
Chairman, Department Committee on Graduate Theses

Tunable Wettability of Microstructured Polypyrrole Films

by

Jean H. Chang

Submitted to the Department of Mechanical Engineering
on August 5, 2010, in partial fulfillment of the
requirements for the degree of
Master of Science in Mechanical Engineering

Abstract

This thesis presents the development of the conducting polymer polypyrrole as a viable material for applications requiring switchable wettability. A fabrication procedure that produces robust microstructured polypyrrole (PPy) that quickly and reversibly switches between the superhydrophobic and superhydrophilic states is discussed. The polymer is doped with perfluorooctanesulfonate ions which diffuse in and out of the film upon an electric stimulus, causing a change in the material's surface energy. The effect of changing different deposition parameters on the switchable wettability of the polymer is also investigated. A post-deposition thermal treatment that improves the electrochemical properties of polypyrrole is presented. Finally, a device that allows for the *in situ* wettability switch of PPy is developed, eliminating the need for polypyrrole to be immersed in an electrolyte in order to switch between wetting states. A wettability gradient created on the surface of PPy using the device is used to demonstrate a possible application requiring induced fluid movement. Electrochemical techniques are used to synthesize and characterize the polymers, and scanning electron microscopy is used to examine the surface morphology of the films.

Thesis Supervisor: Ian W. Hunter
Title: Hatsopoulos Professor of Mechanical Engineering

Acknowledgments

First, I would like to thank my advisor Professor Ian Hunter for his invaluable guidance throughout this project. Many thanks go to the BioInstrumentation Lab polymer group: Dr. Cathy Hogan, Kerri Keng, Eli Paster, Priam Pillai, and Bryan Ruddy. Their ideas, advice, and encouragement have been incredibly helpful throughout this project.

I would also like to thank my colleagues in the BioInstrumentation Lab: Yi Chen, Brian Hemond, Scott McEuen, and Adam Wahab for always being there to bounce around ideas. I am lucky to have worked with such talented people. Thanks to Kate Melvin for her constant positive attitude.

Thank you to the Institute of Soldier Nanotechnologies and the Intelligence Advanced Research Projects Activity for providing funding for this project.

I would like to thank my UROPs, Katie Dalrymple and Abismael Diaz for helping me with the thermal treatment experiments.

Thank you to my best friends, the 'Braintrust,' who are always there to support me in the good times and bad.

Thank you to my siblings: my sister Kathy, whose footsteps I followed throughout elementary, middle, and high school, and my little brother David who shares my interest in engineering. And finally, I would like to thank my parents, Woo Taek and Sook Hee, who always encouraged me to do what I enjoyed. They have provided unconditional support for everything I have pursued.

Contents

List of Figures

List of Tables

Chapter 1

Introduction

1.1 Motivation

Conducting polymers are a promising class of materials that posses unique properties that allow them to be used in a wide variety of applications. In particular, polypyrrole (PPy) is one of the more useful conducting polymers due to its high conductivity (on the order of 10^4 S/m) and stability in ambient conditions. PPy is currently being developed as artificial muscle actuators [17, 38], flexible electrodes [3, 45], sensors [6], supercapacitors [32], battery electrodes [42], microfluidic pumps [34], and cell and tissue culture platforms [63]. Recently, PPy has been shown to switch wetting states upon an electric stimulus [58].

Special surfaces that have the ability to switch between wetting states are of great interest due to their potential applications in lab-on-a-chip devices, cooling systems, smart fabrics, low friction surfaces, and water harvesting. By controlling the surface energy of a material, wettability gradients can be used to induce fluid movement. While there are several methods of switching wettability currently in development, such as electrowetting or photo-, pH-, or thermal-responsive materials, they each have their own set of limitations (discussed in Section 1.3). This thesis focuses on developing polypyrrole as a viable material with switchable wettability and maximizing the capabilities of PPy such that the material can be used as a suitable alternative that addresses the limitations of other switchable materials.

1.2 Wetting

The wettability of a surface is determined by the material's surface energy. A droplet placed on a substrate forms a spherical cap at equilibrium with a contact angle θ_E (see Figure 1-1). Gravity is negligible and the behavior of a droplet is dominated by capillary forces when the droplet radius is less than the *capillary length*, κ^{-1}, given by:

$$\kappa^{-1} = \sqrt{\frac{\gamma_{lv}}{\rho g}} , \tag{1.1}$$

where γ_{lv} is the liquid-vapor interfacial tension of the probe fluid, ρ is the density of the fluid, and g is the gravitational acceleration. The capillary length of water at standard temperature and pressure is 2.7 mm.

A force balance of the three interfacial tensions (liquid-vapor, solid-vapor, solid-liquid) acting on the line of contact (or triple line), yields Young's relation [66]:

$$\gamma_{lv} \cos\theta_E = \gamma_{sv} - \gamma_{sl} , \tag{1.2}$$

where γ is the interface tension between the three phases (solid, liquid, gas). A surface with a water contact angle greater than 90° is called hydrophobic, while surfaces with water contact angles less than 90° are hydrophilic.

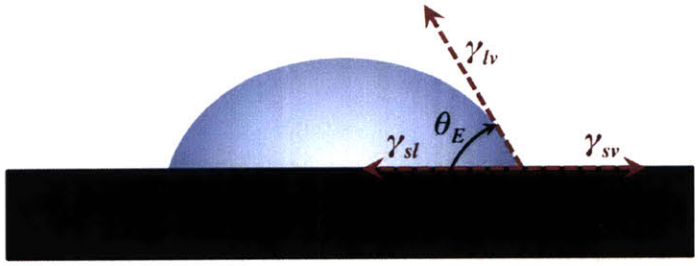

Figure 1-1: A droplet forms a contact angle with a surface.

Young's relation refers to an ideal, flat, chemically homogenous surface. Droplets placed on a textured surface have an *apparent* contact angle θ^* that is different than the *equilibrium* contact angle θ_E of a droplet placed on a flat surface with the same chemical composition. The wetting of rough surfaces was modeled by Wenzel [61],

who found that for a rough surface γ_{sv} and γ_{sl} are magnified by a factor of r, defined by:

$$r = \frac{\text{real surface area}}{\text{projected surface area}} , \tag{1.3}$$

since the surface area of the solid has increased by this amount. The Wenzel model can be derived by considering a small displacement dx of the line of contact (see Figure 1-2). The total change in energy dE per unit length of the triple line becomes:

$$dE = r(\gamma_{sl} - \gamma_{sv})dx + \gamma_{lv}dx\cos\theta^* , \tag{1.4}$$

where r is defined by (1.3). Minimizing E gives the equilibrium condition and we are left with Wenzel's relation in (1.5):

$$\cos\theta^* = r\cos\theta_E . \tag{1.5}$$

It can easily be seen than for $r = 1$, (1.4) will yield Young's relation (1.2). Wenzel's model shows that for a rough surface, where $r > 1$, the surface roughness will amplify the inherent hydrophobicity or hydrophilicity of the material. Specifically, $\theta^* > \theta_E$ for a hydrophobic material where $\theta_E > 90°$, and $\theta^* < \theta_E$ for a hydrophilic material where $\theta_E < 90°$.

Wenzel's model assumes that the droplet is in complete contact with the solid underneath it (Figure 1-3). However, for very rough surfaces (*e.g.* surfaces with roughness on two length-scales, such as the Lotus leaf in Figure 1-4), the Cassie-Baxter state [13] becomes more energetically favorable as air pockets form underneath the droplet and the droplet sits on a composite of solid and air, a phenomenon called the *Lotus leaf effect* (Figure 1-3) [26]. The Cassie-Baxter model describes droplet behavior on a chemically heterogenous substrate, and can be derived by considering the change in energy associated with a small displacement dx of the triple line (Figure 1-2):

$$dE = f_1(\gamma_{sl} - \gamma_{sv})_1 dx + f_2(\gamma_{sl} - \gamma_{sv})_2 dx + \gamma_{lv}dx\cos\theta^* , \tag{1.6}$$

where f_1 and f_2 are the fractional surface areas of the two species. By minimizing E

to obtain the equilibrium condition and applying Young's relation, we are left with the Cassie-Baxter relation:

$$\cos\theta^* = f_1 \cos\theta_1 + f_2 \cos\theta_2 \ , \tag{1.7}$$

where θ_1 and θ_2 are the equilibrium contact angles of species 1 and 2, respectively. It can be seen from (1.7) that the apparent contact angle, θ^*, of a droplet in the Cassie-Baxter state is a weighted average of the equilibrium contact angles of the two species.

If species 1 is solid and species 2 is air, then f_1 and f_2 can be denoted as Φ_s (the fraction surface area of the solid in contact with the droplet) and $1 - \Phi_s$, respectively. Then, $\theta_1 = \theta_E$ and $\theta_2 = \pi$ and (1.7) is reduced to:

$$\cos\theta^* = -1 + \Phi_s(\cos\theta_E + 1) \ . \tag{1.8}$$

It can be seen from (1.8) that when $\Phi_s \ll 1$, θ^* approaches 180°. Thus, superhydrophobic surfaces (where $\theta^* > 150°$) exhibit behavior described by the Cassie-Baxter relation, where air pockets are trapped underneath the droplet.

With non-ideal surfaces that are rough, chemically heterogeneous, or both, a phenomenon called *contact angle hysteresis* is observed. When a droplet is placed on such a surface, the static contact angle will take a value that is between the *advancing* angle, θ_A and the *receding* angle, θ_R. θ_A refers to the maximum contact angle that is observed before the triple line advances when fluid is added to the droplet, and θ_R refers to the minimum contact angle that is observed before the triple line recedes when fluid is removed from the droplet. Contact angle hysteresis is the difference between θ_A and θ_R. Droplets in the Wenzel state are highly pinned and exhibit high contact angle hysteresis while droplets in the Cassie-Baxter state exhibit very low pinning and low contact angle hysteresis (less than 10°).

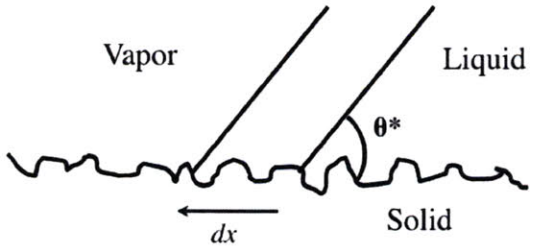

(a) Wenzel model derivation

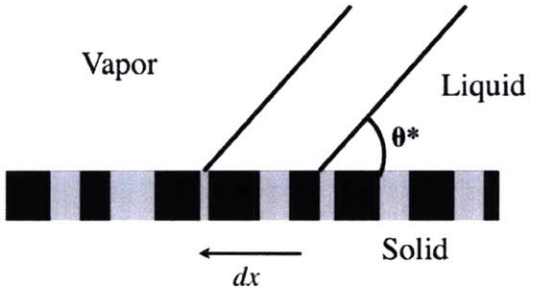

(b) Cassie-Baxter model derivation

Figure 1-2: The Wenzel and Cassie-Baxter models describe wetting on rough surfaces. Figures modified from [22].

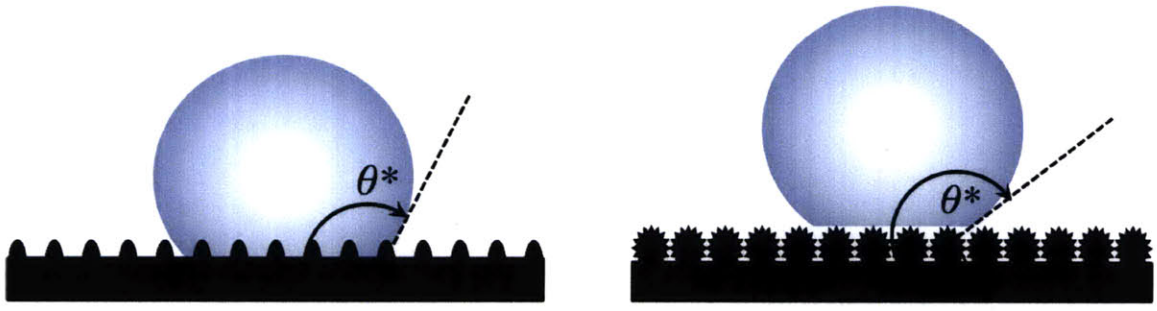

(a) (b)

Figure 1-3: Droplet in the (a) Wenzel state and (b) Cassie-Baxter state, or *fakir* droplet.

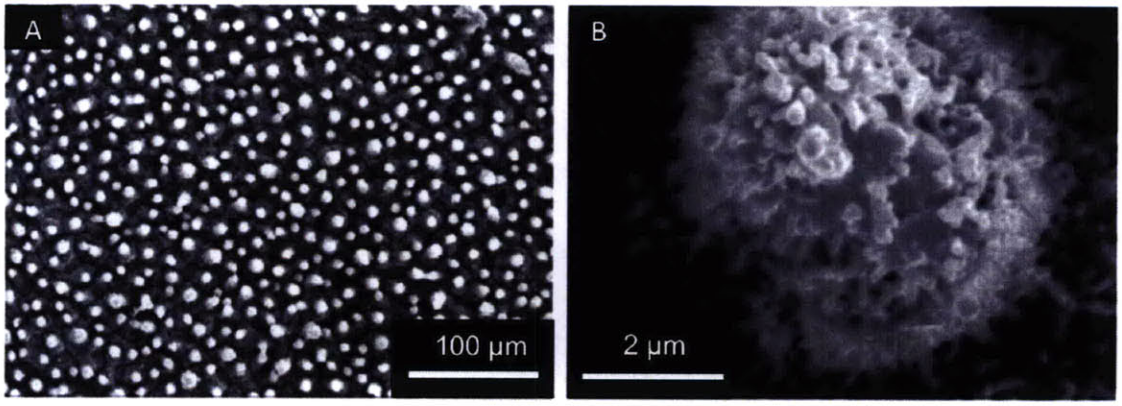

Figure 1-4: The Lotus leaf has both microscale and nanoscale roughness. From [55].

1.2.1 Methods of Measuring Contact Angles

The most common methods of measuring contact angles are by goniometry or Wilhelmy balance tensiometry (WBT). In goniometry, the sessile drop technique is employed where a droplet is placed on a substrate and the contact angle is measured manually or by image analysis (Figure 1-5). To measure contact angle hysteresis, either the captive-drop goniometric (CDG) or the tilting-plate goniometric (TPG) methods are employed. In CDG, a syringe is used to either add to or remove fluid from the droplet and θ_A and θ_R are measured immediately before the triple line moves. In TPG, a droplet is placed on the substrate and the substrate is tilted. θ_A is measured from the leading edge and θ_R is measured from the trailing edge of the droplet immediately before the droplet rolls off the surface. Goniometric techniques have measurement errors of $\pm 2°$. In WBT, a thin plate is oriented perpendicular to the fluid-air interface and the wetting forces are measured as the plate is immersed into or emersed from the fluid (Figure 1-6).

In this thesis, static contact angles were measured using the sessile drop technique. A Canon EOS 50D digital SLR camera with a Canon MP-E 65 mm 1–5× macro lens was used to photograph the droplets and a custom-written MATLAB® script (Appendix A) was used to assign the tangent line. The roll-off angle, α, the angle at which a droplet placed on a substrate begins to roll off was determined to measure the contact angle hysteresis. A 5 µL droplet of deionized water was used as the

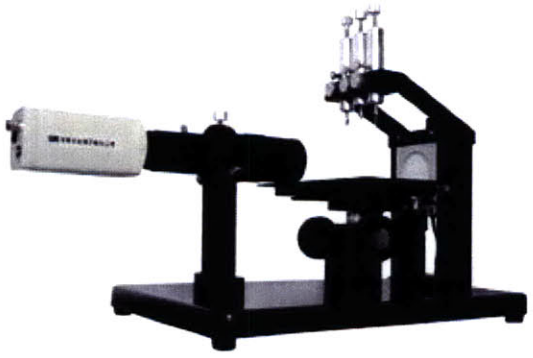

Figure 1-5: A contact angle goniometer. From [57].

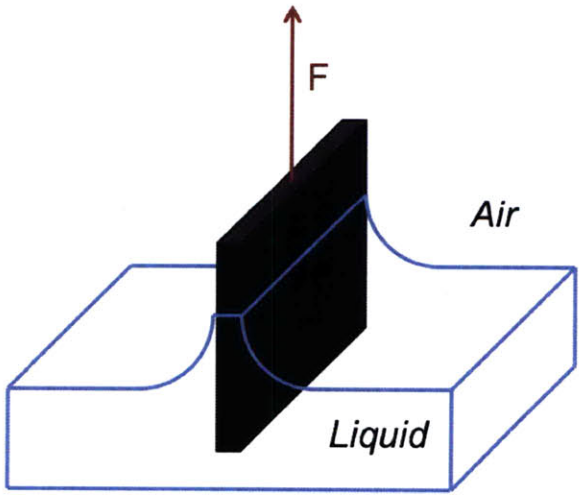

Figure 1-6: Schematic of Wilhelmy-balance tensiometry.

probe fluid, and a tilting stage was used to measure the roll-off angle (Figure 1-7). The relationship between the roll-off angle and contact angle hysteresis can be derived by balancing the capillary and gravitational forces acting on the droplet. The relationship was derived by Furmidge [25] and is given by:

$$\frac{mg(\sin\alpha)}{w} = \gamma_{lv}(\cos\theta_R - \cos\theta_A) \ , \tag{1.9}$$

where mg is the weight of the droplet and w is the width of the droplet projected onto the image plane. Surfaces with low contact angle hysteresis (*i.e.* superhydrophobic surfaces) have low roll-off angles (less than 10°).

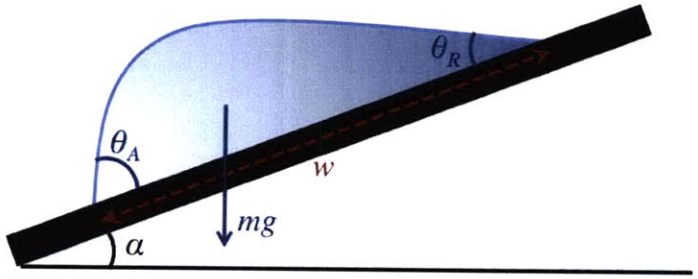

Figure 1-7: The roll-off angle is related to the contact angle hysteresis of a surface. Figure modified from [25].

1.3 Methods of Tuning Wettability

A well-studied method of switching wettability is electrowetting, where an electric field is applied between the fluid and the material. The electric field lowers the surface tension of the fluid and causes a decrease in the contact angle [7, 36]. The switch is fast (on the order of milliseconds) and precise, however electrowetting typically requires high voltages (greater than 100 V). Furthermore, at high voltages, contact angles have been observed to plateau between 30° and 80° depending on the system [41]. Electrowetting methods have recently been employed in lab-on-a-chip applications to move droplets along arbitrary paths and promote chemical reactions by micro-mixing [19, 51], and in optical applications where the droplet is a variable focal length lens [8].

Studies on photo-responsive materials have become more common in recent years. Inorganic semiconductor oxides such as TiO_2, ZnO, and V_2O_5, and organic compounds such as azobenzene have been known to exhibit a reversible light-induced transition between two states [64]. Feng, *et. al* [24] created ZnO nanorod films that reversibly switched from the superhydrophobic to superhydrophilic state upon exposure to ultraviolet light. Unfortunately, photo switches are slow (2 hours for the ZnO films in [24]), and a return to the superhydrophobic state requires several days in the dark (7 days for the films in [24]).

Thermally responsive materials [21, 28] are an attractive method of tuning surface wettability due to the non-contact nature of the switch. Sun, *et. al* [56] reported a nanostructured surface modified by the thermally responsive poly(N-isopropylacrylamide) that was reversibly switched between superhydrophobic (contact angle of 149°) and superhydrophilic (contact angle of 0°) states. Thermal switches, however, tend to be slow, and such materials tend to require a constant thermal stimulus as surfaces return to their original wettability state when heat is removed.

Solvent responsive materials, such as pH-responsive materials, have also been reported. Jiang, *et. al* [31] reported a rough gold substrate that was modified with 1-(11-mercaptoundecanamido)benzoic acid that was reversibly switched between the superhydrophobic (contact angle of 155°) and superhydrophilic (contact angle of 0°) states when exposed to fluids with different pH values. However, the requirement of contact the surface with a chemical limits the applications for such materials.

A wettability switch can also be induced by a microscale change in the surface morphology. Chen, *et. al* [18] fabricated a metal/polymer composite membrane with an array of hydrophobic microposts which were deflected by an electrostatic force. They were able to achieve a contact angle range of 131° to 152°.

In addition to the discussed limitations, all of the above-mentioned materials require complex fabrication methods. They require a micro- or nano-structured surface (created often by hard-template methods) modified by the stimuli-responsive material in order to achieve a switch between the superhydrophobic and superhydrophilic states.

1.3.1 Polypyrrole as a Material with Tunable Wettability

PPy offers many advantages over the methods and materials mentioned in Section 1.3 due to its low operation voltage (typically less than 5 V), fast electrochemical switch (on the order of minutes), and its relative ease of fabrication (no need for micro-fabrication processes). In addition, PPy is extremely stable and does not require a continuous energy input in order to operate — if the applied voltage is removed it does not revert back to its original wetting state until another voltage is applied.

PPy's unique properties come from its microstructure, in which the dopants are contained within a network of polypyrrole chains rather than becoming a part of the polymer's molecular structure (Figure 1-8). This allows for dopants to be easily incorporated into and released from the polymer. By applying a voltage and oxidizing/reducing the film, the chemical composition of the polymer can be altered, changing the surface energy of the material.

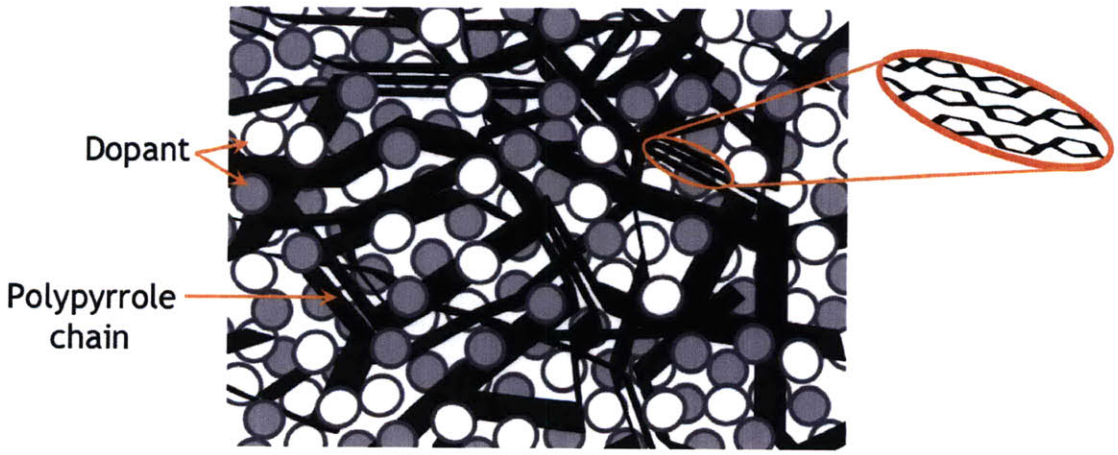

Figure 1-8: PPy microstructure. Figure modified from [44].

The diffusive elastic model (DEM) developed by J. Madden [39] describes the change in the chemical composition of PPy upon an electric stimulus (Figure 1-9). In the DEM, a PPy film is placed in an electrochemical cell which consists of a working electrode (the PPy film), a counter electrode, a reference electrode, and an electrolyte solution, and a voltage is applied between the polymer and counter electrode. Current flows through the electrolyte and ions at the polymer surface begin

charging the electrochemical double layer capacitance, changing the ion concentration at the surface as positive or negative ions become attracted to or repelled from the charge. This difference in ion concentration drives the diffusion of ions into or out of the polymer, resulting in a change in the chemical composition.

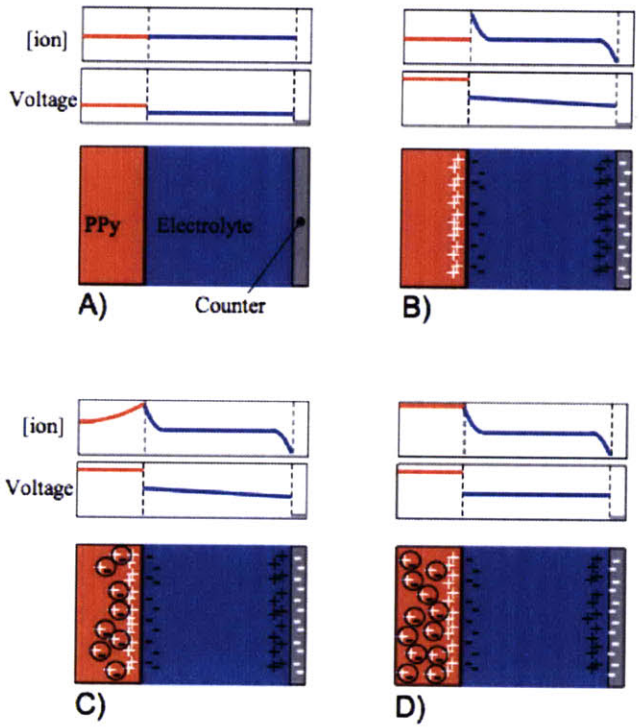

Figure 1-9: The diffusive elastic model. (A) Voltage applied. (B) Charging of the double layer capacitance. (C) Double layer charge drives diffusion of ions into or out of polymer. (D) Electric current in the polymer flows to balance charge. Figure modified from [40].

1.4 Description of Chapters

Chapter 2 describes the fabrication process for growing robust PPy films that can be reversibly switched between the superhydrophobic and superhydrophilic states. The effect of changing different recipe parameters is explored, and an optimal recipe that produced PPy films with the least degradation with cycling is presented.

Chapter 3 reports the effects of a low-temperature thermal treatment on the switch-

able wettability of PPy.

Chapter 4 describes the process for fabricating the encapsulated device that allows for the *in situ* wettability switch of PPy. Various substrates as well as different electrolyte recipes are investigated.

Chapter 5 presents a proof-of-concept device for potential applications requiring induced fluid movement. A possible filtering application for oil-water separation is also explored. Areas for future development are presented.

Chapter 6 gives a brief summary of the work presented in this thesis.

Chapter 2

Template-free Synthesis of Textured Polypyrrole Films

It is well known that an electrical stimulus will change the doping state of conducting polymers. The change in dopant state corresponds to a change in the chemical composition of the material and can cause a volumetric expansion or contraction. The surface energy can therefore be controlled. This chapter describes the development of a fabrication protocol for polypyrrole films with reversible, switchable wettability, and discusses the effects of changing the deposition parameters.

2.1 Previous Work on Superhydrophobic Conducting Polymer Surfaces

A textured surface is required to achieve a superhydrophobic state, which can be realized either by hard-template or template-free methods. This section focuses on groups that were able to attain a reversible wettability switch of PPy.

Wang, *et. al* [60] employed a hard-template method of creating a structured polypyrrole surface, and were able to achieve a contact angle range of 44° to 129°. The polymer was doped with dedecylbenzenesulfonic acid and the wettability was switched by immersing the material in an aqueous electrolyte (0.1 M sodium dode-

cylbenzenesulfonate, or NaDBS) and applying an oxidizing or reducing voltage.

Template-free methods of creating structured superhydrophobic conducting polymers have also been reported [59]. Although the micro/nanostructure size and the surface morphology is less controllable than hard-template methods, the ease of fabrication makes template-free methods highly desirable. Xu, *et. al* [65] reported a facile template-free method of creating superhydrophobic PPy surfaces with switchable wettability, achieving a large contact angle range, between 0° and 152°.

Another template-free method of creating superhydrophobic PPy is to modify the chemical structure of pyrrole. Darmanin and Guittard [20] synthesized polypyrrole with both superhydrophobic and superoleophobic properties by flourinating the pyrrole monomer.

2.2 Polypyrrole Polymerization

PPy can be polymerized either chemically or electrochemically. The polymerization process as described by Baker and Reynolds [4] is shown in 2-1. The polymerization process involves the removal of electrons via either a catalyst (chemical polymerization) or an electrode (electrochemical deposition).

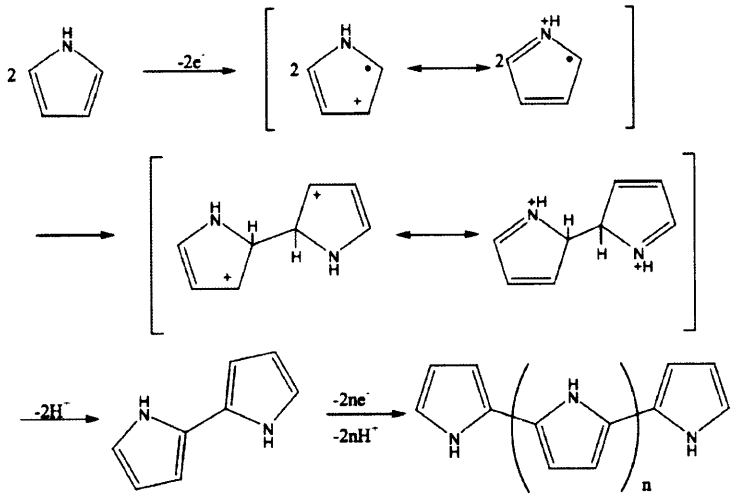

Figure 2-1: Polypyrrole synthesis. Figure modified from [39].

It has been reported that combining the chemical and electrochemical polymeriza-

tion of PPy by adding a catalyst (*i.e.* ferric chloride, or $FeCl_3$) to the electrochemical deposition setup will yield rough PPy films [65]. The presence of Fe^{3+} ions oxidize a small amount of the pyrrole in solution resulting in a suspension of PPy clusters on the order of tens of micrometers, while the driving current polymerizes the PPy clusters at the working electrode. This results in a network of rough microstructures on top of a smooth layer of PPy on the working electrode.

To maximize the range of potential applications for which polypyrrole can be used, the material should be able to switch quickly and reversibly between the superhydrophobic and superhydrophilic states. The deposition protocol presented in [65] was modified and optimized to yield robust superhydrophobic PPy films with fast switching times. The electrochemical bath used for deposition, shown in Figure 2-2 was constructed out of Teflon® and contained a 25 mm × 25 mm × 3 mm glassy carbon working electrode (WE) and gold-coated stainless steel foil as the counter electrode (CE). The glassy carbon was positioned horizontally to allow for the uniform growth of the PPy microstructures on the surface of the electrode, and was affixed to the Teflon® bath with a PTFE-filled Delrin clamp. When the working electrode was positioned vertically, it was found that due to gravity, a thicker layer of microstructures grew towards the bottom of the electrode resulting in a wettability gradient, as shown in Figure 2-3 (less hydrophobic towards the top of the electrode). The gradient was eliminated by positioning the WE horizontally. Electrical contact with the WE was made with a screw that contacted the bottom of the WE. A silicone gasket was used to prevent the deposition solution from leaking out the bottom of the bath.

Pyrrole (Sigma-Aldrich, 98%) was vacuum-distilled and stored at -20°C. Potassium perfluorooctanesulfonate (Sigma-Aldrich), iron (III) chloride hexahydrate (ferric chloride) (Sigma-Aldrich), and acetonitrile (anhydrous, 99.8%) (Sigma-Aldrich) were of analytical grade and used as received. The deposition solution contained 0.1 M pyrrole, 0.015 M KPFOS, and 0.0008 M $FeCl_3$ in acetonitrile, and the ingredients were vigorously mixed for 30 minutes to allow for PPy clusters to form in solution. The concentration of $FeCl_3$ was kept low to ensure that the polymer was doped primarily with $PFOS^-$ ions. The solution was then added to the electrochemical deposition

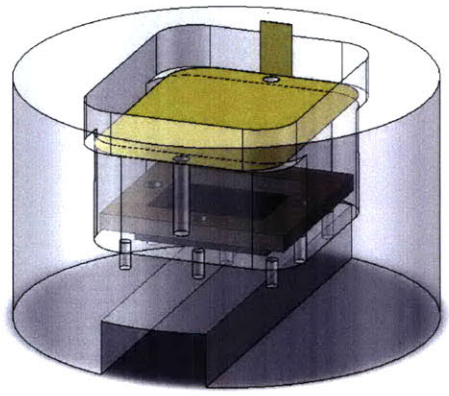

(a) Isometric view

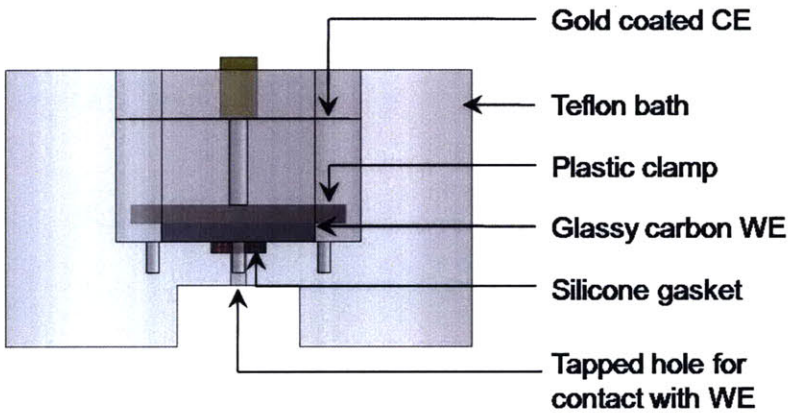

(b) Side view

Figure 2-2: Electrochemical deposition bath

(a) PPy film grown on vertically positioned glassy carbon WE.

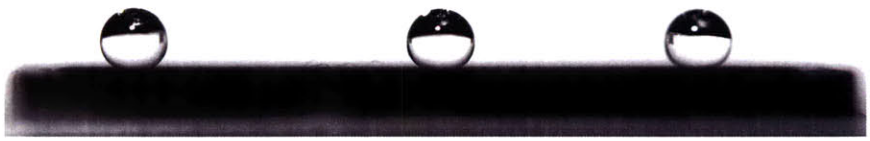

(b) PPy film grown on horizontally positioned glassy carbon WE.

Figure 2-3: Gravity causes a thicker layer of microstructures to grow towards the bottom of the working electrode when the electrode is positioned vertically in the electrochemical deposition cell, resulting in a wettability gradient.

bath and PPy was grown galvanostatically with current density of 1.5 A/m^2 for two hours at ambient temperature. The current density was applied using a VMP2 Multichannel Potentiostat with EC-Lab software. The film was rinsed with acetonitrile and allowed to air dry. The resulting PPy film had a hierarchal surface roughness and was superhydrophobic with a contact angle of up to 164° (Figure 2-4). A view of the film edge shows that the PPy film consists of a thin smooth film with a network of rough microstructures that have grown on top of the thin film (Figure 2-5). A KLA Tencor P-11 Surface Profiler with a 2 μm diamter stylus was used to measure the film thickness and surface roughness. The underlying thin film was measured to be 178 nm thick while the rough microstructures were measured to be 15-30 μm thick. The average surface roughness was measured to be 4.13 μm.

The presence of ferric chloride in the deposition solution allowed for the template-free synthesis of superhydrophobic PPy [65]. A PPy film grown with the same deposition solution and under the same deposition conditions except for the omission of ferric chloride was very smooth and lacked the secondary network of microstructures. The resulting film (Figure 2-6) was slightly hydrophilic with a contact angle of 84° and had a cauliflower structure that is typical of galvanostatically-deposited PPy [44]. The average surface roughness, S_a, was measured to be 0.432 μm, an order of magnitude less than S_a of the superhydrophobic PPy.

Other probe fluids were tested and the contact angles of these fluids on the superhydrophobic PPy are shown in Table 2.1. The polymer exhibited high repellency (high contact angles) to high surface tension fluids such as glycerol. Low surface tension fluids such as propylene glycol completely wetted the surface. The polymer exhibited superoleophilic properties as oil completely wetted the surface. The polymer showed high hydrophobicity to salt water with salinity comparable to seawater (0.6 M NaCl in H_2O) with a contact angle of 142°. However, as the concentration of NaCl in the aqueous solution increased, the contact angle decreased linearly (Figure 2-7).

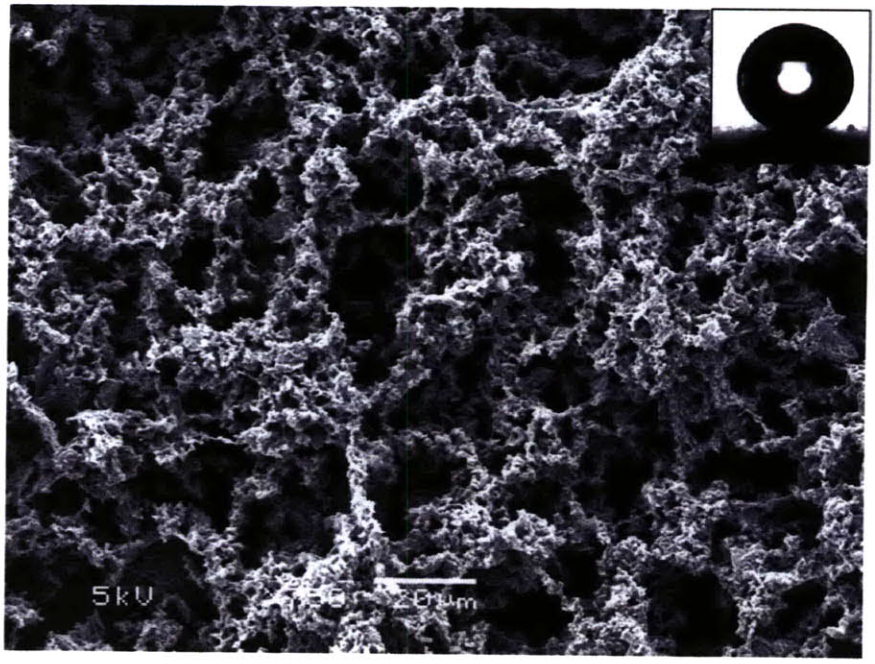

(a)

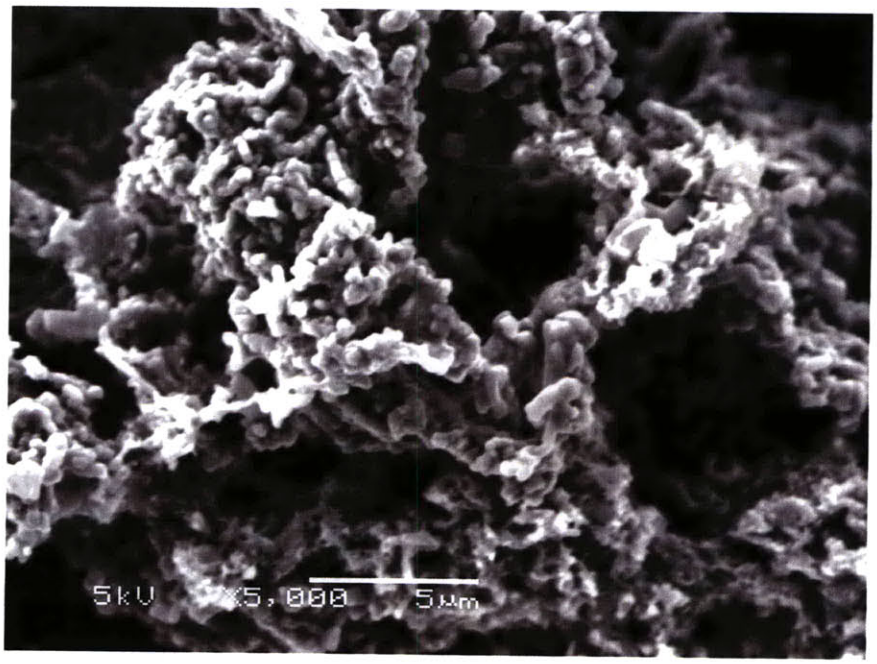

(b)

Figure 2-4: Scanning electron microscopy (SEM) micrographs of superhydrophobic PPy. The polymer has a roughness on two length scales.

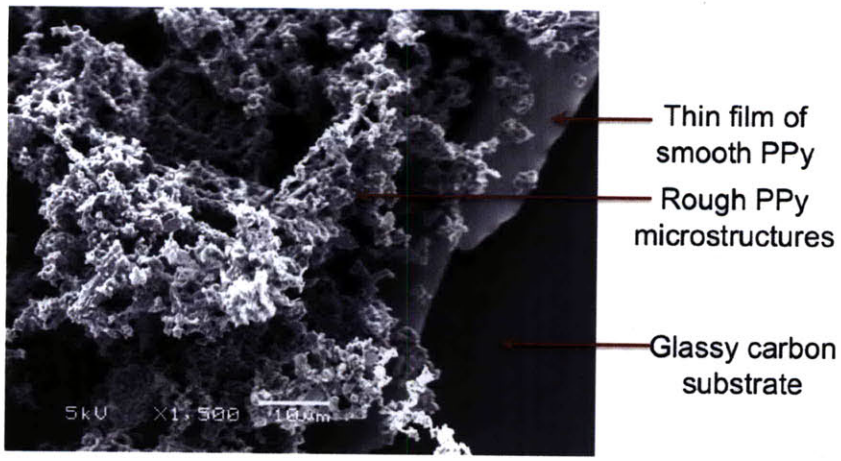

Figure 2-5: Film edge

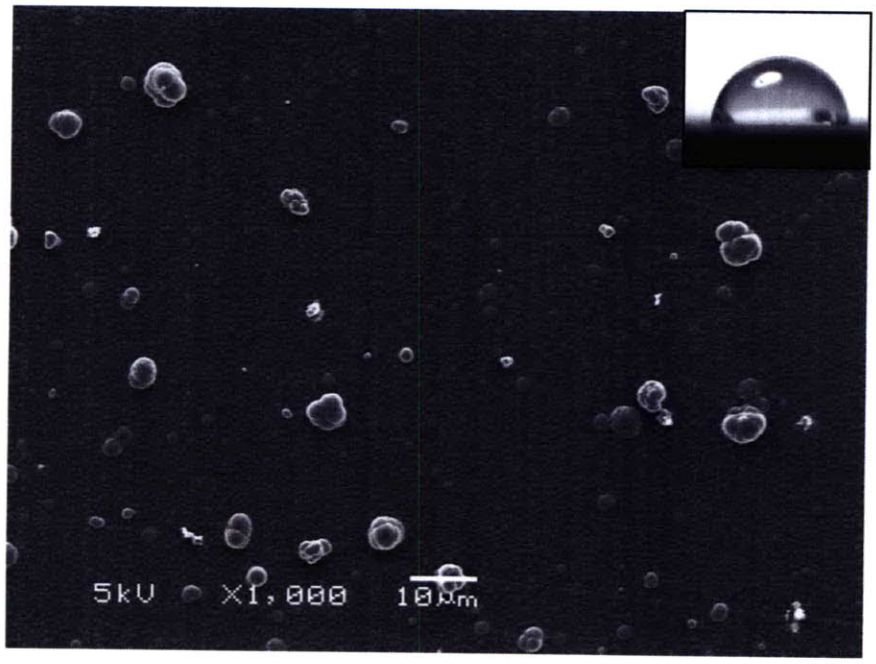

Figure 2-6: A PPy film grown without $FeCl_3$ lacked the secondary network of microstructures and had a contact angle of 84°.

Table 2.1: Contact Angles of Different Probe Fluids

Name	Surface Tension, γ_{lv}, at 20°C (mN/m)	Contact Angle (°)
Water	72.8	164
Glycerol	64.0	146
Ethylene glycol	47.7	51
Propylene glycol	38.0	0
Oil	20-25	0
6.0 M NaCl in water	82.55	76

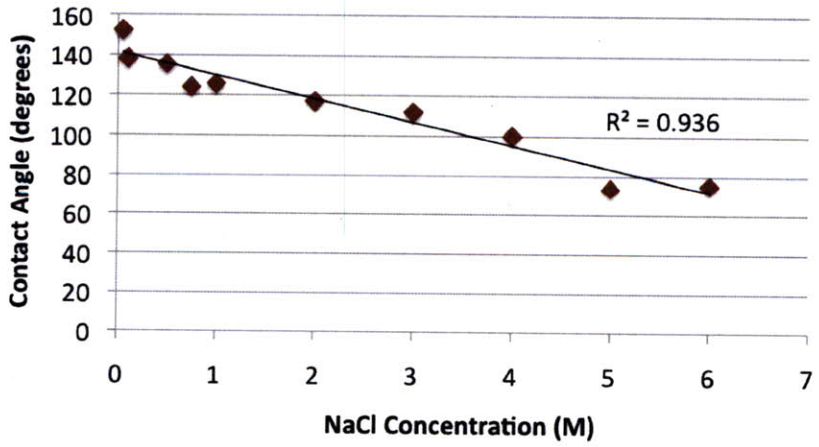

Figure 2-7: Contact angle plotted as a function of NaCl concentration in H_2O.

2.3 Electrochemically-induced Wettability Switch

As mentioned previously in Section 1.3.1, the wettability of PPy can be switched by electrically inducing a change in the chemical composition of the material (Figure 2-8). The initial state of the as-deposited polymer is superhydrophobic since it is doped with the low surface-energy perfluorooctanesulfonate ($PFOS^-$) ion. When a negative voltage is applied with respect to the reference electrode (or counter electrode in a two-electrode configuration), the film is reduced as $PFOS^-$ ions are driven out of the material. PPy in the undoped state is inherently hydrophilic, and thus the reduced film is superhydrophilic due to its surface roughness. Oxidizing the film by applying a positive voltage reverses the switch resulting once again in a superhydrophobic film. Intermediate wetting states can be achieved by leaving the material in a partially doped state.

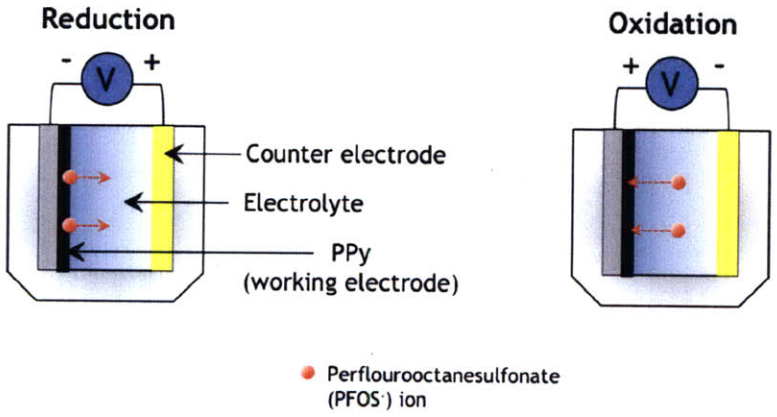

(a) Schematic of oxidation/reduction process

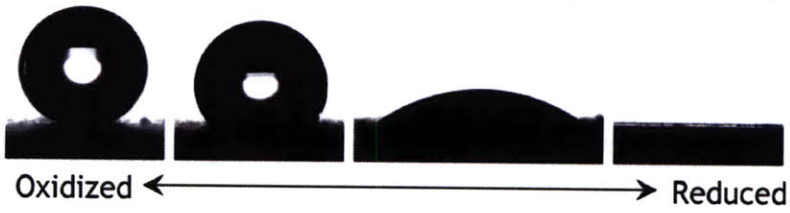

(b) PPy wetting states

Figure 2-8: Different wetting states can be achieved by oxidizing or reducing PPy.

A JEOL 6700F scanning electron microscope was used to perform electron dispersive spectroscopy (EDS) on the polymer in the oxidized and in the reduced state.

EDS revealed the presence of fluorine ions in the hydrophobic, oxidized polymer, and no fluorine ions in the hydrophilic, reduced polymer, indicating that it is in fact the diffusion of the $PFOS^-$ ions in and out of the polymer that caused the wettability switch, rather than the reorientation of $PFOS^-$ ions inside the polymer (Figure 2-9).

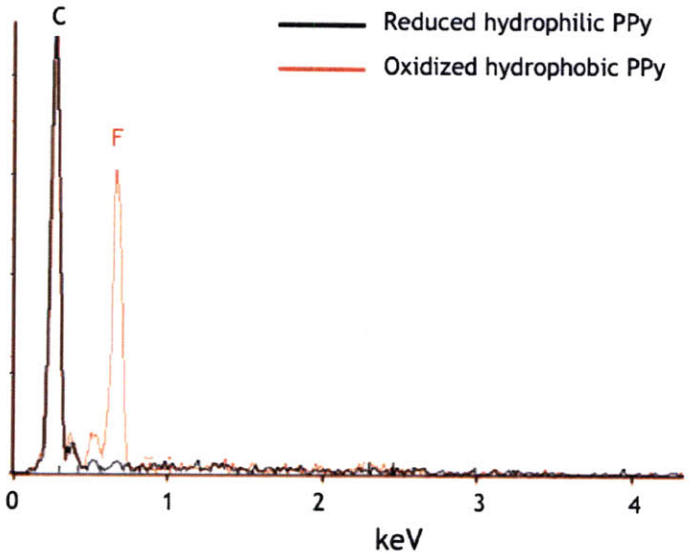

Figure 2-9: EDS spectra of oxidized and reduced PPy.

An electrochemical switching cell was constructed out of Teflon® to perform the electrochemical wettability switch. The cell contained a gold-coated stainless steel foil as the counter electrode and an Ag wire reference electrode (RE). PPy grown on a glassy carbon electrode was used as the working electrode. The electrolyte switching solution contained 0.015 M KPFOS in acetonitrile.

The polymer was reduced by applying a voltage of -0.6 V with respect to the Ag RE. It was observed that the initial state of the polymer was over-doped, and a threshold of charge (-1072 $\pm$ 225 C/m^2) that diffused out of the film needed to be reached before the material could quickly switch between wetting states. Thus, the first reduction cycle (2 minutes) was much longer than subsequent reduction cycles.

The polymers grown with the deposition protocol described in Section 2.2 had much faster switching times than polymers grown by Xu, *et. al* [65]. After the first reduction cycle which allowed for the threshold of charge to be reached, the polymer

switched from the superhydrophobic to superhydrophilic state in 30 seconds, a forty-fold decrease in the switching time when compared to the switching time (20 minutes) of the polymers reported in [65]. The switching time can be increased by increasing the applied voltage, but -0.6 V was chosen to compare with the polymers grown with the deposition procedure in [65]. The polymer was oxidized by applying a voltage of +0.6 V with respect to the Ag RE, and switched back to the superhydrophobic state after five minutes, a four-fold decrease in the oxidation time of the polymers reported in [65]. The difference in the oxidation and reduction times can be attributed to the reduced polymer being less conductive than the oxidized polymer.

2.3.1 Cycling Experiments

A cycling experiment was performed to determine the reversibility of the film over a number of cycles. For the first reduction, -0.6 V with respect to the Ag RE was applied for two minutes to allow for the charge threshold to be reached. A positive (+0.6 V with respect to the Ag RE for five minutes) and negative (-0.6 V with respect to the Ag RE for 30 seconds) voltage were alternated for the subsequent oxidation/reduction cycles. The current across the working and counter electrodes was measured to monitor the charge transfer (Figure 2-10). Contact angles of the film in the oxidized and reduced states were measured after ten, 50, and 100 cycles (Figure 2-11).

A drop in the hydrophobicity of the film after the first cycle was observed. This may be due to the polymer being over-doped in its initial state after deposition, as it is difficult to drive all of the ions back into the polymer. There was also a slight drop in hydrophobicity over the course of the experiment, which can be attributed to damage to the microstructures when handling the material (*i.e.* when transferring the film in and out of the electrolyte solution to take measurements).

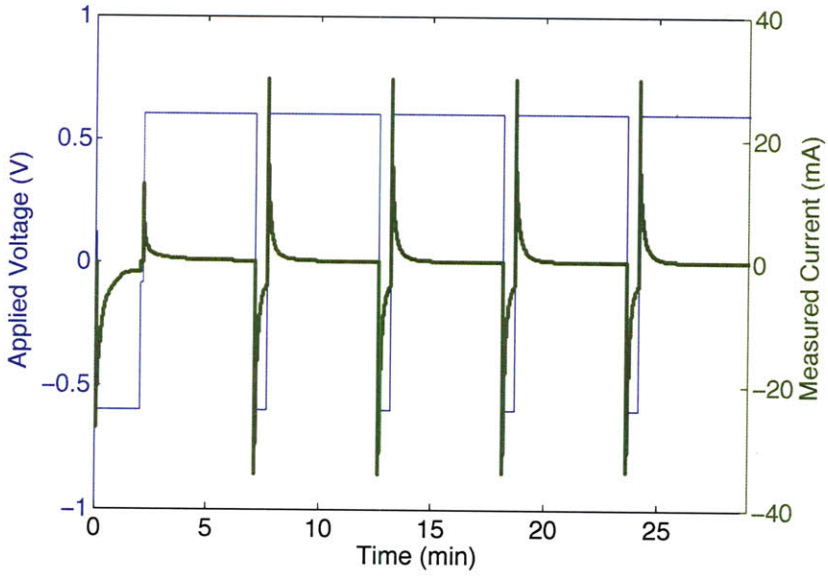

Figure 2-10: First five cycles of cycling experiment.

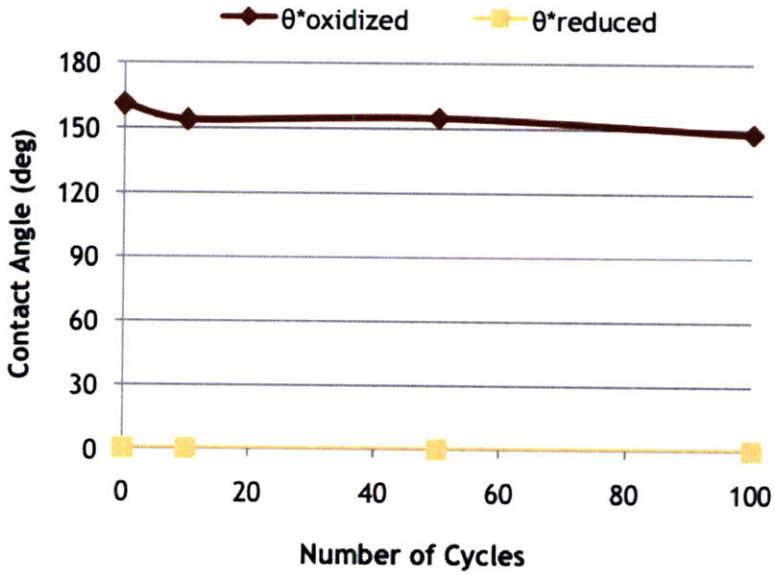

Figure 2-11: The polymer lasts at least 100 cycles, but experiences a slight decrease in hydrophobicity due to damage to the microstructures.

2.4 Effect of Deposition Parameters on Reversible Wettability

2.4.1 Current Density

PPy films were grown with the same deposition solution as the procedure described in Section 2.2 galvanostatically at current densities ranging from 0.5 A/m^2 to 2.5 A/m^2 for two hours, at ambient temperature. SEM images revealed that the higher the current density, the denser the network of microstructures (Figure 2-12). Surface profilometer scans showed that both the thickness of the underlying smooth film and the microstructure network increased with current density (Table 2.2).

Table 2.2: Thicknesses of Films Grown at Different Current Densities

Current Density (A/m^2)	Underlying Film Thickness (nm)	Microstructure Thickness (μm)
0.5	50	10-25
1.0	70	10-25
1.5	178	15-30
2.0	180	25-40
2.5	160	35-40

Reversibility experiments were performed on the films grown at different current densities (Figure 2-13). The contact angle hysteresis before and after cycling was measured by the roll-off angle of a 5 μL droplet for each of the films grown at the different current densities (Figure 2-13). The initial roll-off angle was lower for the films grown at the lower current densities, because there was less solid (lower Φ_s) in contact with the droplet and therefore less contact line pinning. There was an increase in the roll-off angle due to damage to the microstructures when handling the material. Small black pieces of polymer approximately tens of micrometers in diameter were found in the switching solution after cycling, indicating that the microstructures have fallen off during the experiment. The maximum contact angle (contact angle of the films in the oxidized state) before and after cycling was also measured. The films

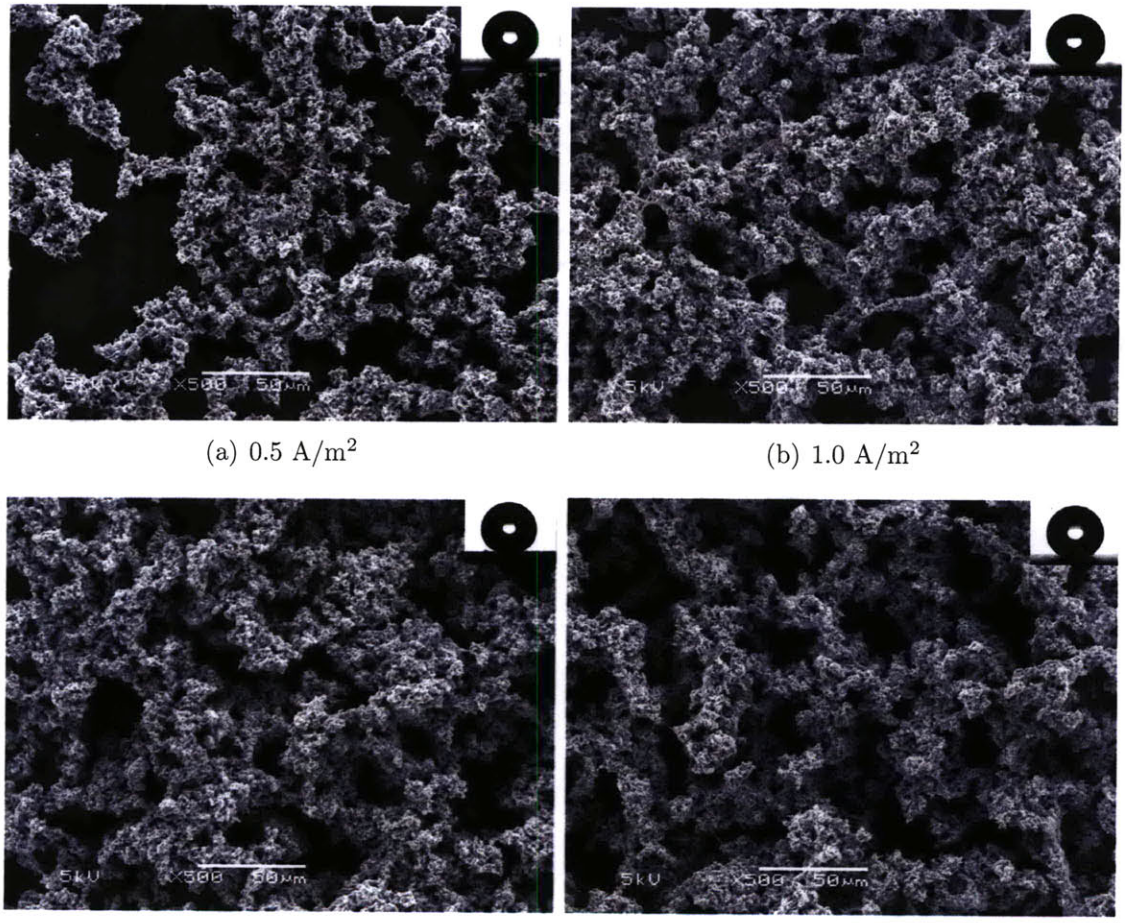

(a) 0.5 A/m^2 (b) 1.0 A/m^2

(c) 2.0 A/m^2 (d) 2.5 A/m^2

Figure 2-12: PPy films grown with 0.1 M pyrrole, 0.0008 M $FeCl_3$, 0.015 M KP-FOS, at different current densities. The films were grown for two hours at ambient temperature.

experienced a drop in hydrophobicity due to the initial state of the polymer being over-doped.

The reversibility experiments showed that the film with the highest initial contact angle and the least degradation after cycling was grown at 1.5 A/m^2, confirming that the deposition protocol in Section 2.2 resulted in films at the optimal current density.

The film grown at 2.5 A/m^2 experienced a large decrease in the maximum contact angle after cycling. There is no data point for the roll-off angle after cycling because 5 μL droplets placed on the film were fully pinned and did not roll off. In addition, the thickness of the film lower than the thickness of the film grown with a current density of 2.0 A/m^2. A current density of 2.5 A/m^2 is therefore too high and damages the polymer during the polymerization process, resulting in a film that does not behave as expected.

2.4.2 $FeCl_3$ Concentration

The concentration of $FeCl_3$ in the deposition solution was changed to determine its effect on the surface morphology as well as the switchable wettability of PPy. The concentration of $FeCl_3$ was reduced by half. The deposition solution contained 0.1 M pyrrole, 0.0004 M $FeCl_3$, and 0.015 M KPFOS in acetonitrile. The films were grown galvanostatically at current densities ranging from 0.5 A/m^2 to 2.5 A/m^2 for two hours at ambient temperature. The resulting films had a thicker underlying film and a less dense network of microstructures than the films grown with 0.0008 M $FeCl_3$. As expected, the thickness of the underlying film and the microstructures increased with current density.

It is thus expected that increasing the concentration of $FeCl_3$ in the deposition solution will result in films with thinner underlying films and a more dense network of microstructures since the deposition will be dominated by the polymerization of the microstructures.

Reversibility experiments were performed on the films grown with 0.0004 M $FeCl_3$. The roll-off angles for a 5 μL droplet before and after cycling were measured to determine the change in contact angle hysteresis, and the contact angles of the oxidized

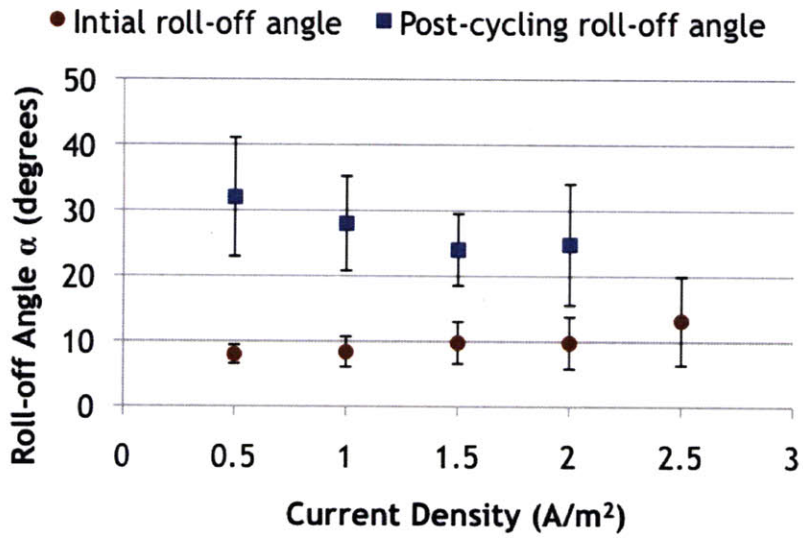

(a) Change in contact angle hysteresis after cycling.

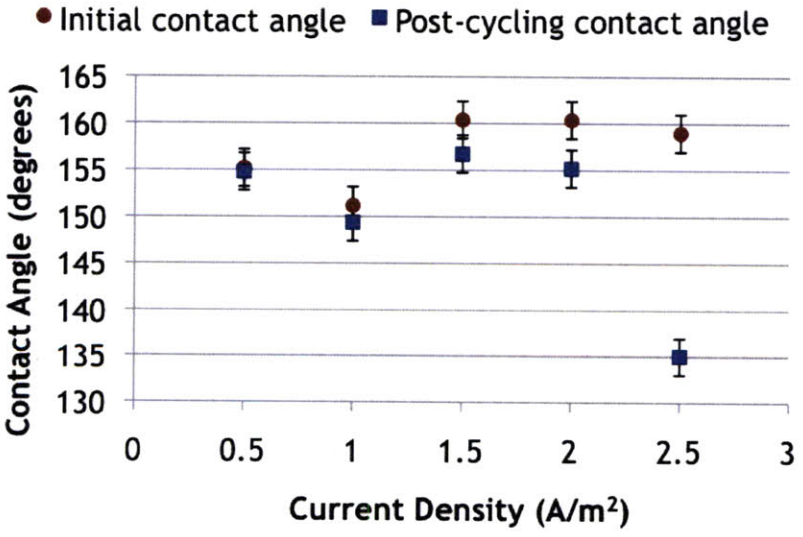

(b) Change in maximum contact angle after cycling.

Figure 2-13: Reversibility experiments of films grown with 0.1 M pyrrole, 0.0008 M $FeCl_3$ and 0.015 M KPFOS in acetonitrile.

film before and after cycling were measured (Figure 2-15). Droplets placed on the film grown at 0.5 A/m^2 were completely pinned and had no roll-off angle, indicating that the microstructure network was too sparse to render the film superhydrophobic. There was also a significant drop in the contact angle of the oxidized film after cycling, from 116° to 23°.

Similar to the films grown with 0.0008 M $FeCl_3$, there was an increase in the contact angle hysteresis in all of the films after cycling. There was also a slight drop in the hydrophobicity of the materials after cycling. Unlike the films grown with 0.0008 M $FeCl_3$, the film grown with 0.0004 M $FeCl_3$ and a current density of 2.5 A/m^2 did not show complete degradation after cycling. The polymer was not damaged during the deposition process.

These experiments show that films grown with 0.0004 M $FeCl_3$ have higher contact angle hysteresis and experience more degradation after cycling when compared to films grown with 0.0008 M $FeCl_3$. In addition, films grown at 2.0 A/m^2 had the least amount of degradation after cycling.

Table 2.3: Thicknesses of Films Grown with 0.0004 M $FeCl_3$

Current Density (A/m^2)	Underlying Film Thickness (nm)	Microstructure Thickness (μm)
0.5	73	3-11
1.0	85	10-25
1.5	193	20-35
2.0	389	30-40
2.5	558	20-30

2.4.3 Dopant

The surface morphology as well as the reversible wettability of PPy is also dependent on the dopant. PPy films grown with a dopant that had the same anion but a different cation than the films grown in Section 2.2 yielded films with an irreversible wettability switch. Films were grown with a deposition solution that contained 0.1 M pyrrole, 0.0002 M $FeCl_3$, and 0.05 M tetraethylammonium perfluorooctanesulfonate

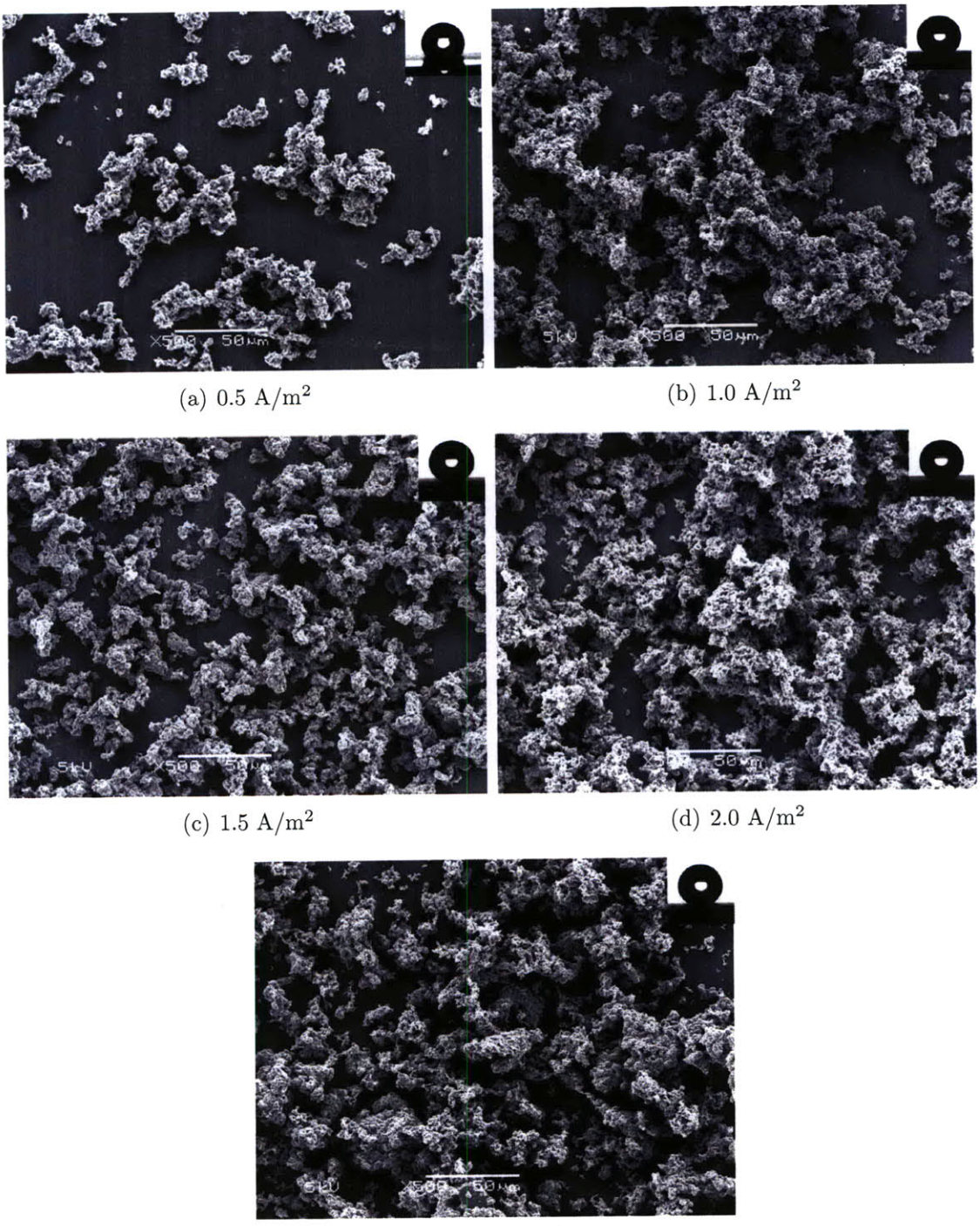

(a) 0.5 A/m^2

(b) 1.0 A/m^2

(c) 1.5 A/m^2

(d) 2.0 A/m^2

(e) 2.5 A/m^2

Figure 2-14: PPy films grown with 0.1 M pyrrole, 0.0004 M $FeCl_3$, 0.015 M KP-FOS, at different current densities. The films were grown for two hours at ambient temperature.

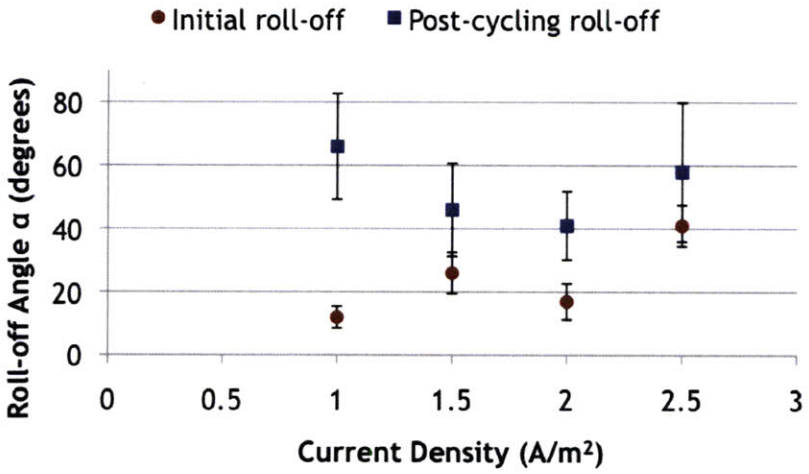

(a) Change in contact angle hysteresis after cycling.

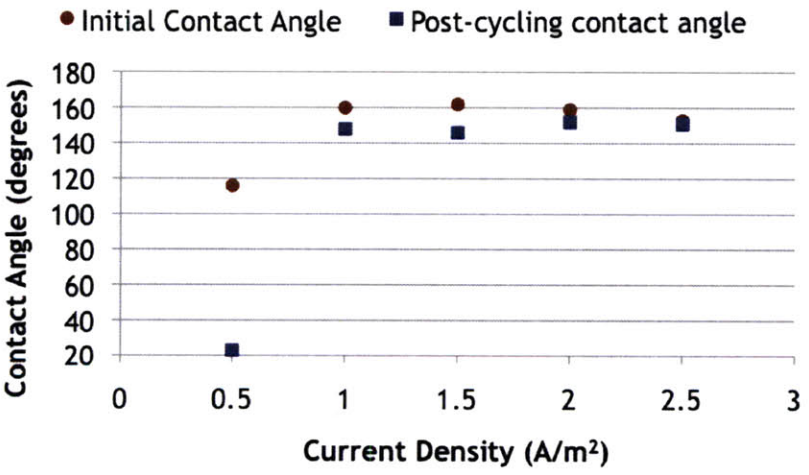

(b) Change in maximum contact angle after cycling.

Figure 2-15: Reversibility experiments of films grown with 0.1 M pyrrole, 0.0004 M $FeCl_3$ and 0.015 M KPFOS in acetonitrile.

in acetonitrile. The films were grown galvanostatically at a current density of 2.5 A/m^2 for one hour at ambient temperature. The initial state of the film was superhydrophobic, and the film was switched to the superhydrophilic state by applying a negative voltage (-0.6 V for 20 minutes). SEM images of the film before and after reduction revealed a mechanical change in the surface features — the reduced film had noticeably smaller grains than the oxidized film (Figure 2-16). The average surface roughness of the reduced film ($S_a = 2.90$ μm) was measured to be 32% less than the average surface roughness of the film in its initial state ($S_a = 4.25$ μm). This indicates that the large cation is diffusing and causing a surface morphology change.

PPy films grown with a slightly smaller anion yielded films with a different surface morphology. Films were grown with the deposition protocol described in Section 2.2, except with 0.015 M potassium nonafluorobutanesulfonate as the dopant. The resulting films (Figure 2-17) were superhydrophobic and were reversibly switched between wetting states, but had a surface morphology that appeared different than the morphology of the film in Figure 2-4.

2.5 Summary

Superhydrophobic PPy films with a fast switching time were grown via a template-free deposition. The deposition recipe utilized ferric chloride as a catalyst to grow a rough network of microstructures on top of the film, allowing droplets placed on the film to be in the Cassie-Baxter state. The films were able to be reversibly switched between the superhydrophobic and superhydrophilic states upon oxidation and reduction, but experienced slight degradation during cycling. The films were able to survive at least 100 oxidation and reduction cycles.

The effects of growing PPy films at different current densities and with a smaller concentration of ferric chloride were also investigated. The contact angle hysteresis and the contact angle of the films in the hydrophobic state were measured before and after cycling. In addition, the effects of changing the dopant on the surface morphology were explored.

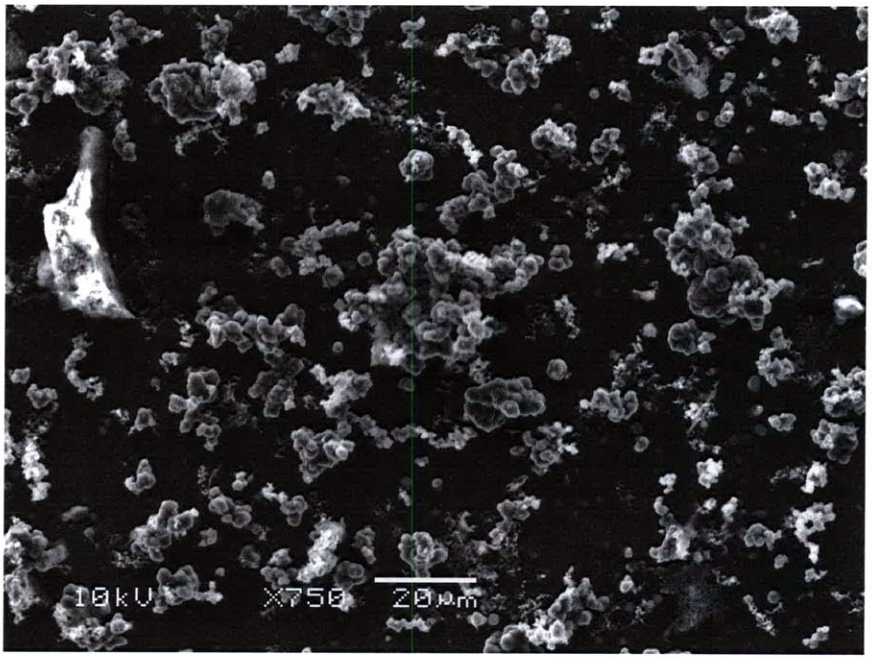

(a) Initial state

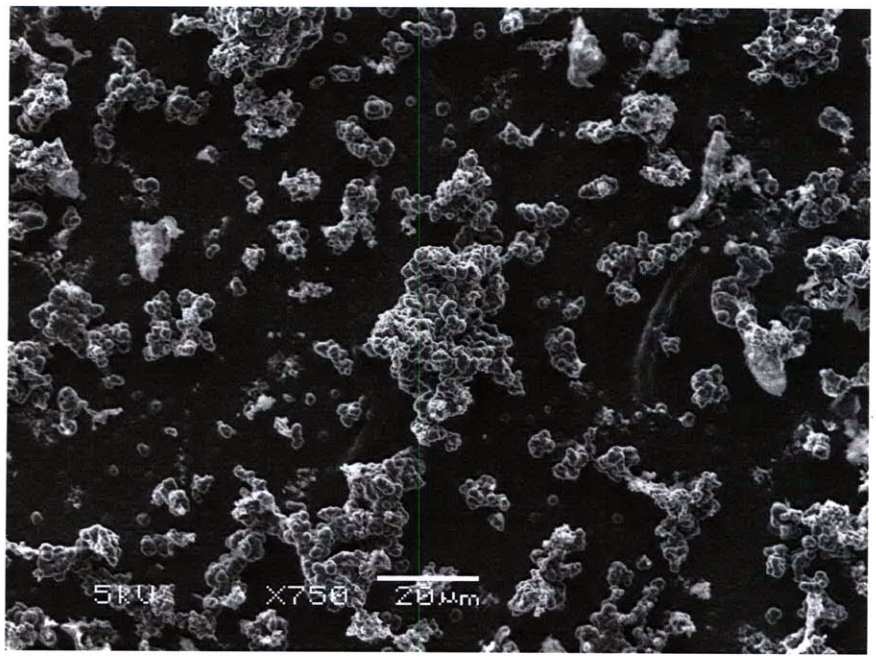

(b) Reduced film

Figure 2-16: PPy doped with tetraethylammonium perfluorooctanesulfonate exhibited a surface morphology change upon reduction.

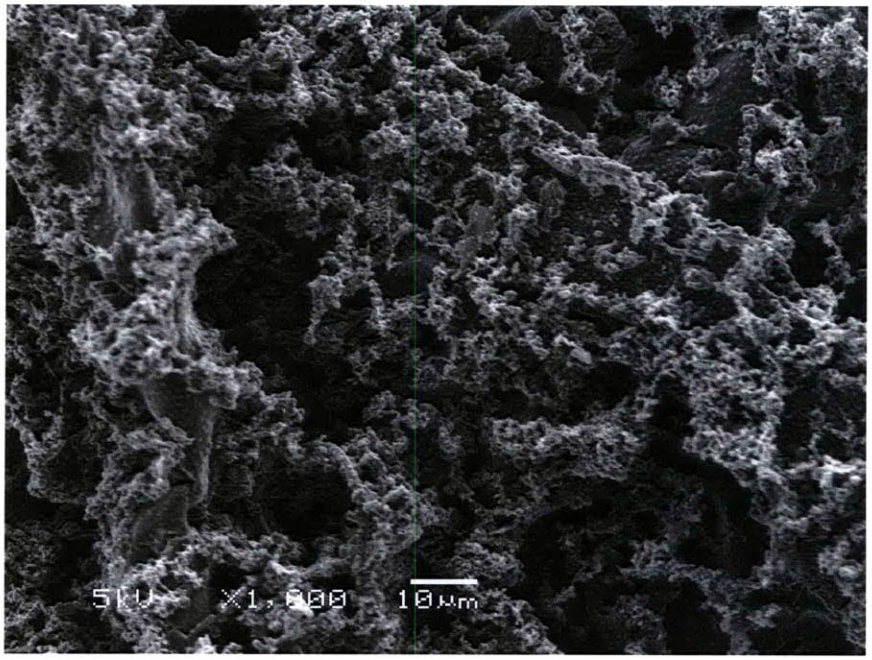

Figure 2-17: PPy with potassium nonafluorobutanesulfonate as the dopant.

Chapter 3

Effect of Thermal Treatment on Switchable Wettability

There have been several studies that investigate the effect of a post-deposition thermal treatment on the conductivity of polypyrrole, but there have been relatively few studies that examine the effects of thermal treatments on the electrochemical properties of PPy. This chapter investigates the effect of a post-deposition baking treatment on the switchable wettability characteristics of PPy.

3.1 Review of Previous Work on PPy Thermal Treatments

Previously studies have shown that the effect of thermal treatments on PPy is dependent on the dopant. Kaynak and Hakansson [33] studied the effect of short-term heat treatments on the conductivity of polypyrrole-coated textiles. The samples were heated to the desired temperature and the temperature was maintained for 900 s before cooling back to ambient temperature. It was found that the resistance of the polymer decreased during the thermal treatment, but either increased or decreased after cooling, depending on the dopant or the temperature of the treatment. Kaynak and Hakansson hypothesized that thermal treatment 'annealed' the polymer by

promoting the growth of ordered, crystalline areas which increased the conductivity.

Ansari and Wallace [2] studied the effect of thermal treatment on the redox activity of polypyrrole chloride (PPy-Cl), polypyrrole dodecylsulfate (PPy-DS), polypyrrole *p*-toluene sulfonate (PPy-PTS), and polypyrrole ferricyanide (PPy-$Fe(CN)_6$). The samples were heated for one hour at temperatures ranging from 100°Cto 300°C, and the conductivities were measured. PPy-Cl experienced too much degradation for adequate conductivity measurements. PPy-DS and PPy-PTS both experienced an increase in conductivity while PPy-$Fe(CN)_6$ exhibited a decrease in conductivity after thermal treatment. Cyclic voltammograms also revealed a change in the electrochemical activity of the polymer after thermal treatment. Ansari and Wallace concluded that the change in conductivity and redox activity is dependent on the dopant, and can either improve or degrade the electroactivity of the polymer.

Chehimi and Abdeljalil [16] used inverse gas chromotography to measure the surface energy of polypyrrole and found that the surface energy of PPy-Cl decreased with increasing treatment time at 150°C. On the other hand, the surface energy of PPy-PTS increased with treatment time up to 3 hours and then decreased with increasing treatment time. Cheah, *et. al* [15] used x-ray diffraction to determine the loss of ordering in the polymer backbone after a long-term (60 days) thermal treatment of PPy doped with 1,5-napthalene disulfonate. Ando, *et. al* [1] reported a drop in the conductivity of PPy doped with ClO_4^- due to the decomposition of the polymer and the loss of the dopant ion with temperature treatments between 150°C and 300°C.

Since the wettability switch of PPy is an electrochemically induced switch, it is thus expected that a thermal treatment will change the switchable wettability characteristics of PPy. However, until now, there have been no studies on the effect of thermal treatments on microstructured PPy doped with $PFOS^-$.

3.2 Post-deposition Baking Treatment

PPy films were grown on glassy carbon electrodes using the deposition protocol developed in Section 2.2. The polymers were baked in a Thermolyne 47900 furnace for

two hours at temperatures ranging from 50°C to 300°C. The polymers were allowed to cool down to ambient temperature and the electrochemical properties were measured.

SEM micrographs of films after the thermal treatment showed extensive structural damage to films baked at 300°C and visible damage to films baked at 200°C (Figure 3-1). The damage to the film baked at 300°C was extensive enough to render the film completely non-conductive and hydrophilic — a droplet placed on the film had a contact angle of 50° ± 2°. Therefore, treatments with temperatures higher than 200°C were not further investigated. Droplets placed on films treated at 200°C were in the Wenzel state and had contact angle of 142° ± 2°. Droplets placed on films treated below 200°C showed no significant decrease in post-treatment contact angle.

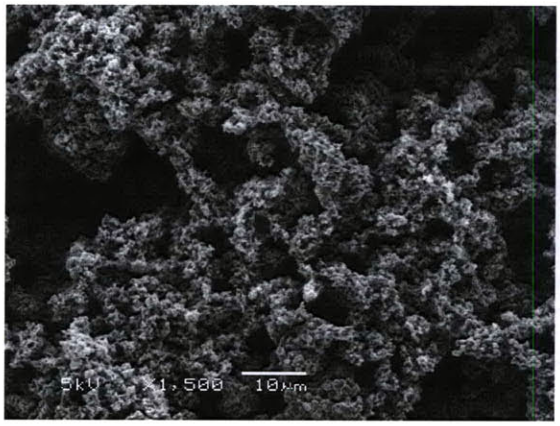

(a) Unbaked film

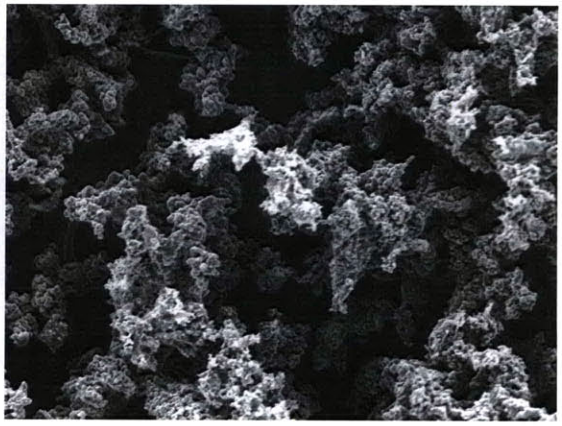

(b) Film baked at 200°C

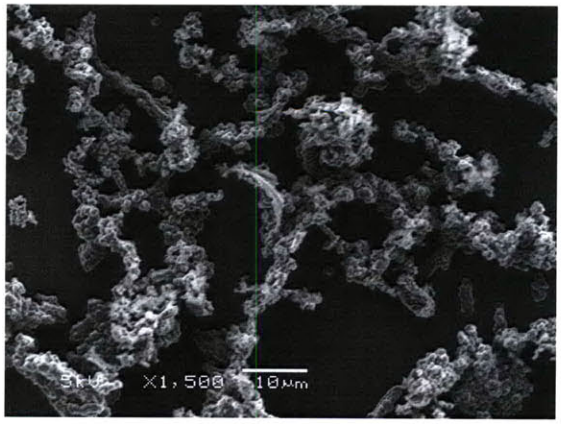

(c) Film baked at 300°C

Figure 3-1: Damage to surface morphology after high temperature thermal treatment.

3.2.1 Charge Threshold

Section 2.3 described a charge threshold that needed to diffuse out of the film before the film could be easily switching between wetting states. A typical plot of an electrochemical wettability switching experiment of an unbaked film is shown in Figure 3-2. The film was grown with the deposition protocol described in Section 2.2. The film was first reduced until the film was converted from a superhydrophobic to superhydrophilic state. A reduction step consisted of applying -0.6 V with respect to an Ag RE for 30 seconds in an electrochemical switching cell. The reduced PPy film was then oxidized until the film was converted back to a superhydrophobic state, with each oxidation step consisting of applying +0.6 V for five minutes. The contact angle as well as the charge transferred was measured after each step, and the contact angle versus the total charge transferred (normalized for the size of the film) is shown in Figure 3-2. The results show that there is a threshold of charge (approximately -950 C/m^2 for this particular film) that needs to diffuse out of the film before the film starts switching between wetting states.

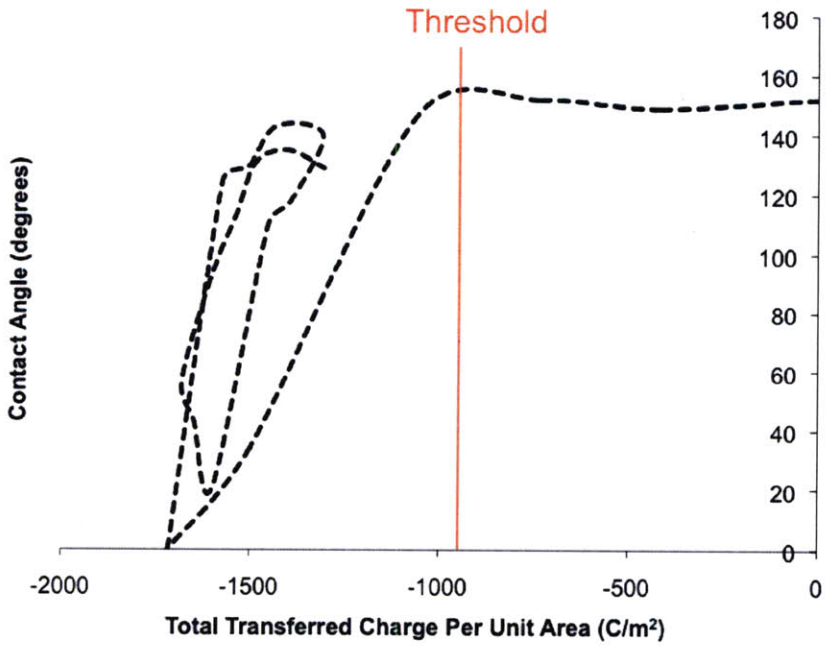

Figure 3-2: A typical plot of an electrochemical wettability switching experiment on an unbaked PPy film.

It was found that baking the PPy films at an elevated temperature decreased the charge threshold. Electrochemical wettability switching experiments were performed on PPy films baked for two hours at temperatures ranging from 50°C to 200°C, and the charge threshold vs. baking temperature was plotted in Figure 3-3. A treatment temperature of 22°C corresponds to the unbaked film.

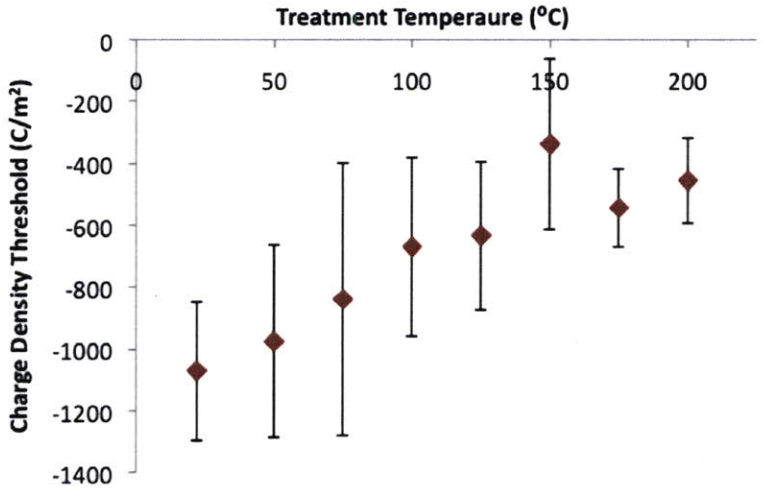

Figure 3-3: Charge density thresholds for PPy films baked at elevated temperatures.

The greatest reduction in charge density threshold occurred for films baked at 150°C. The threshold was reduced to 228 ± 276 C/m^2. Baking at temperatures above 150°C resulted in an increase in the charge density threshold, and may correspond to polymer degradation. The large ranges for the error bars may be due to variability in depositions between samples, and due to the inexact (discretized, rather than continuous) method of determining the threshold value.

3.2.2 Cyclic Voltammograms

Cyclic voltammograms were performed on the treated PPy films between -0.8 V and +0.8 V at a scan rate of 25 mV/s. The results, with the first cycle omitted, are shown in Figure 3-4. The voltage was measured versus an Ag RE. As the treatment temperature increased, the electrochemical activity of the polymer decreased as there was less current measured across the working electrode and counter electrode. For

films treated at temperatures up to 150°C, there was an oxidation peak that existed between +0.4 V and +0.5 V. There was no apparent reduction peak, which may mean that the reduction peak is outside the voltage window. However, when the voltage window was increased to ±1.0 V, there were current spikes at the voltage extremes, indicating that the electrolyte was degrading.

The cyclic voltammograms of the films baked at 175°C and 200°C show decreased electrochemical activity after each cycle, indicating that the electrochemical process is no longer reversible. The films became less capacitive after each cycle as they were losing their ability to store ions. The films baked at 175°C and 200°C were irreversibly damaged by the temperature treatment.

3.2.3 Discussion

The optimal temperature at which to bake the films and achieve the largest decrease in charge density threshold was found to be 150°C. Films baked above this temperature exhibited poor electrochemical properties (*i.e.* capacitance) due to thermal degradation. The decrease in charge density threshold can be due to several different mechanisms. The baking treatment may have evaporated any residual solvent or moisture in the film. The latter is more likely, since acetonitrile's low flash point (6°C) causes quick evaporation of the solvent at room temperature. Since the deposition is not conducted in a dry nitrogen chamber, any humidity present in the ambient surroundings may have become incorporated into the film.

Other possible reasons for the decrease in charge density threshold may be due to the change in the molecular structure of either the dopant or the polymer. It is unlikely that the dopant degraded as the treatment temperatures were much lower than the decomposition temperature of $PFOS^-$ (390°C). The polymer may have degraded slightly at temperatures less than 150°C such that the structure decomposed slightly such that amount of dopant that needed to diffuse out of the film before the polymer became hydrophilic decreased. The slight decomposition of the polymer may not have been severe enough for a noticeable change in the apparent morphology or a significant change in the electrochemistry of the material. Further testing, such as

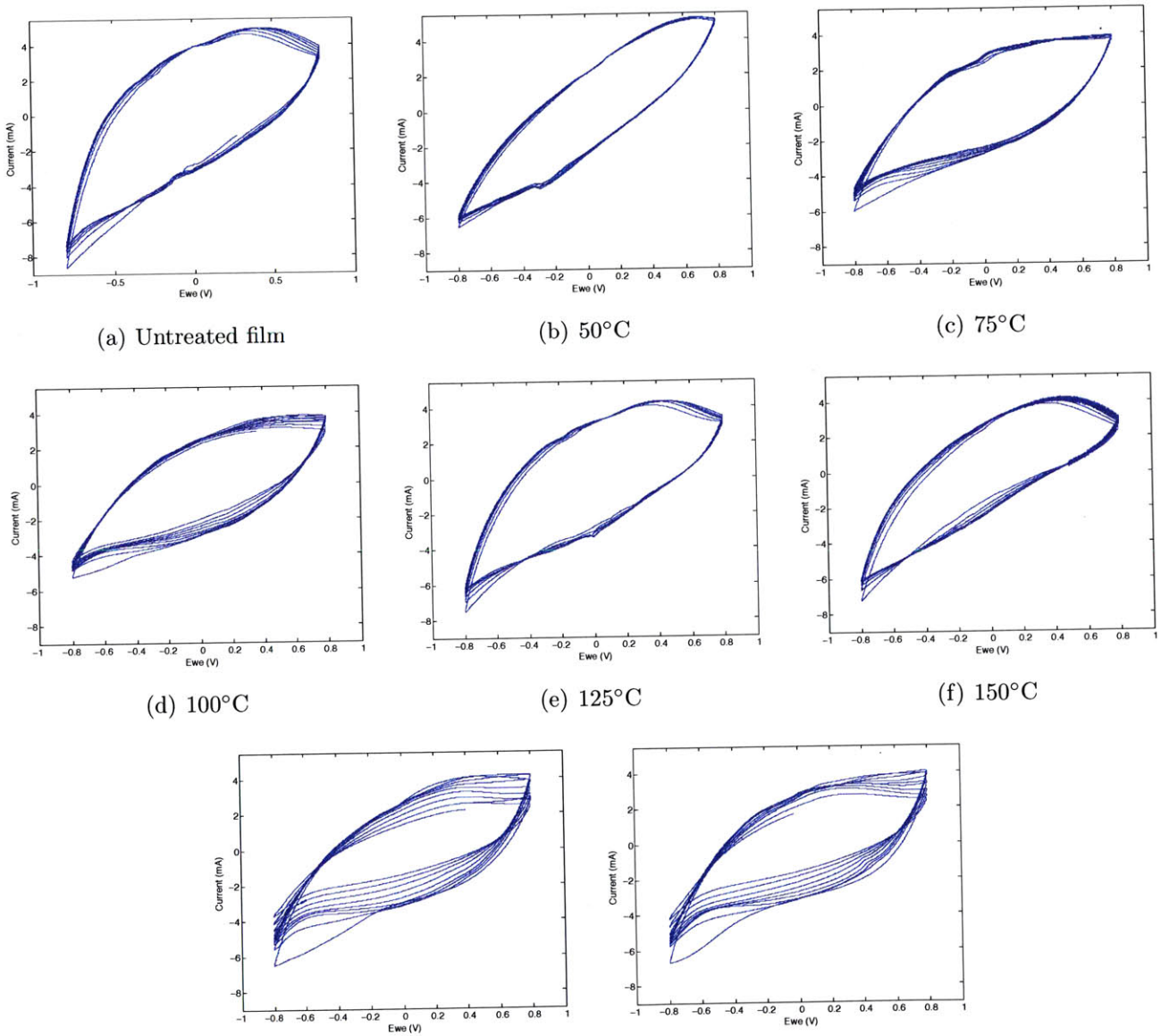

(a) Untreated film (b) 50°C (c) 75°C

(d) 100°C (e) 125°C (f) 150°C

(g) 175°C (h) 200°C

Figure 3-4: Cyclic voltammograms of baked films.

x-ray diffraction microscopy, can confirm whether PPy undergoes a structural change during the temperature treatment.

Chapter 4

Development of In Situ Wettability Switch

The usefulness of the switchable wettability of PPy have been limited due to the requirement of immersion in electrolyte in order to facilitate the switch. An *in situ* wettability switch, where the wettability is switched while a probe droplet is sitting on the surface, is important for fine-tuning the surface energy of the material. In addition, the elimination of the electrolyte immersion requirement opens the door for PPy to be used in a wide variety of applications. The achievement of an *in situ* wettability switch allows for PPy to compete with other previously described methods of tuning wettability.

This chapter describes the development of a device that allows for the *in situ* wettability switch of polypyrrole.

4.1 Review of Previous Work on the *In Situ* Wettability Switch of PPy

Only a few groups have been able to achieve the *in situ* wettability switch of PPy, and they have reported a limited range of contact angle values. Causley, *et. al* [14] reported the induced movement of electrolyte solution through a microchannel coated

with polypyrrole doped with dodecylbenzenesulfonate (PPy-DBS). The channel was immersed in an aqueous electrolyte containing 0.1 M potassium chloride (KCl), and when a voltage was applied, a wettability gradient inside the channel was creating, resulting in the movement of the KCl solution further into the channel. The same group reported more recently the controlled transport of dichloromethane through a platinum mesh coated with PPy-DBS [27]. The mesh was immersed in an aqueous solution containing 0.1 M sodium nitrate ($NaNO_3$). Dichloromethane (DCM) drops adopted a spherical cap shape with a contact angle of 120° when placed on the coated mesh, and underwent a shape transformation when the polymer was reduced allowing for the passage of the DCM drops through the mesh. Liu, *et. al* [37] also reported the *in situ* wettability switch of a 1,2-dichloroethane droplet on a PPy-DBS film. The polymer was immersed in an aqueous solution containing 0.1 M lithium perchlorate, and the contact angle of a 1,2-dichloroethane droplet was switched between 117° and 149° upon the application of an oxidation or reduction potential. Although these groups have achieved an *in situ* wettability switch of PPy, they needed to immerse the polymer in electrolyte which severely limits the applications for which the polymer can be used. The polymer will always need to be in an electrolyte environment and only probe fluids that are immiscible with the electrolyte can be used.

Isakkson, *et. al* reported a device that was able to electrochemically switch the wettability of polyaniline, another conducting polymer, doped with dodecylbenzenesulfonate, and reported the directional spreading of a droplet on an electrochemically induced wettability gradient [29, 30]. The group was able to switch the wettability of the polymer without immersion in electrolyte, but reported only a limited range of contact angle values, 9° to 37°. To date, there has been no group that has been able to switch the wettability of polypyrrole without immersion in electrolyte. The following sections describe the development of a device that allows for the *in situ* wettability switch of PPy without immersion in electrolyte. The device was able to achieve a full range of contact angles by switching the polymer from a superhydrophobic to a superhydrophilic state.

4.2 Concept

The concept for the *in situ* wettability switch was to create a switching device that acted as a 'portable electrochemical cell.' The device consisted of an electrolyte layer sandwiched between a PPy layer which acted as the WE and a gold-coated stainless steel foil that acted as the CE. When a negative voltage is applied, $PFOS^-$ ions will travel from the surface through the bulk polymer material and into the electrolyte layer, switching the PPy to a hydrophilic state (Figure 4-1). The polymer can be switched back to a hydrophobic state by applying a positive voltage and driving the ions back into the polymer. An example of a switching device used during experiments in shown in Figure 4-2.

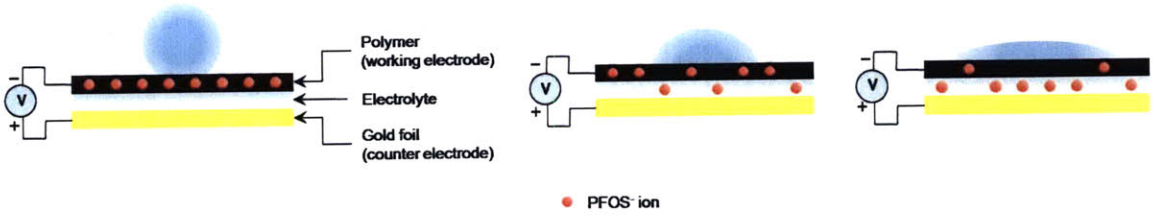

Figure 4-1: Schematic for switching device. When a voltage is applied, the wettability of the polymer is changed as ions travel from the surface of the polymer to the electrolyte layer.

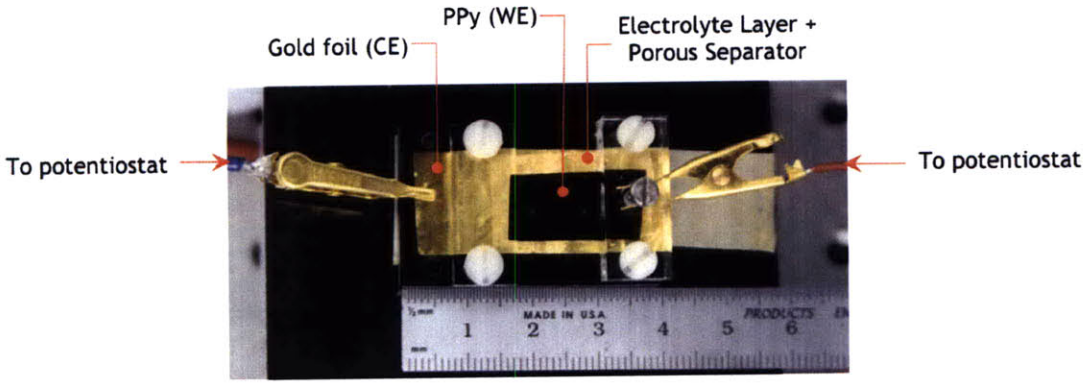

Figure 4-2: Switching device used for experiments.

4.3 Fabrication of Polypyrrole Layer

Previously, when the polymer was grown on top of the substrate and the polymer was switched in an electrochemical switching cell, the ions traveled directly from the surface of the film to the electrolyte. However, in the *in situ* switching device, the ions need to travel though the bulk polymer material to the electrolyte, so it cannot be grown on top of a substrate. The PPy layer must either be free-standing or grown on a porous substrate.

4.3.1 Free-standing PPy Film

A free-standing film was grown by first growing a thick layer of smoother PPy on a glassy carbon substrate and then grown the microstructured superhydrophobic PPy on top of this layer. The smooth PPy was grown with a deposition solution that contained 0.015 M KPFOS and 0.1 M pyrrole in acetonitrile. The film was grown galvanostatically with a current density of 1.5 A/m^2 for four hours at 4°C. The film was grown at a cold temperature to allow for the growth of a highly smooth film that was able to be peeled off the substrate. Superhydrophobic PPy was then grown on top of the smooth film using the procedure described in Section 2.2.

The free-standing film was fragile and required great care during the peel-off step of the fabrication process and when handling the material. It was thus determined that the polymer should be grown on a porous substrate for mechanical robustness. In order for the $PFOS^-$ ions to diffuse from the surface to the electrolyte, the polymer needs to be continuous throughout the porous substrate, that is to say, the polymer needs to grow within the pores of the substrate to bridge together the two sides of the substrate.

4.3.2 Filter Paper Substrate

Polyvinylidene flouride (PVDF) filter paper with 0.45 μm pores (Immobilon-P Transfer Membrane from Millipore Corporation) was initially selected as the porous substrate. This filter paper is used as the substrate in the fabrication of polypyrrole

trilayer actuators. The substrate was made conductive by sputter coating both sides of the substrate with 60 nm of Au using a Desk II Sputter Coater.

To prevent a roughness-induced wettability gradient as discussed in Section 2.2, a deposition bath that positioned the filter paper substrate horizontally was used. However, positioning the substrate horizontally and depositing polymer on both sides caused some polypyrrole to grow around air bubbles and deposit on the underside of the substrate. Only some of the polymeric bubbles subsequently collapsed, resulting in the formation of large (100-500 μm) bubble features on the underside of the substrate, shown in Figure 4-3. Due to the undesirable bubble topography as well as leakage issues, a deposition bath that positioned the filter paper substrate vertically was used instead. Since a porous substrate is much rougher than a glassy carbon substrate, the resulting polymer was much rougher and therefore less sensitive to gravity-induced roughness gradients.

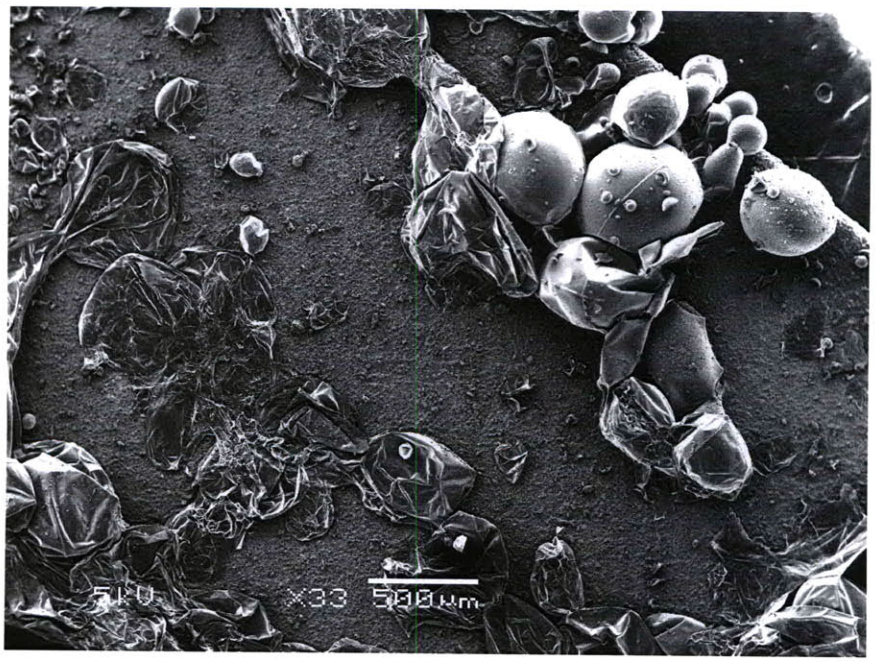

Figure 4-3: Polymeric bubbles formed on the underside of a horizontally positioned filter paper substrate.

Superhydrophobic PPy was grown on both sides of the PVDF filter paper, however the substrate was too thick (113 μm) for the PPy that grew in the pores to bridge a connection between the two sides of the substrate. PVDF filter paper was therefore

deemed an unsuitable substrate.

Lens Paper

Lens paper was selected as a substrate because it was porous, lint-free, and thin (25–30 μm). A metal-free deposition protocol was investigated to determine whether PPy with switchable wettability could be grown on non-conductive substrates. The deposition protocol can be described in three steps: (1) electroless deposition of PPy, (2) electrochemical deposition of smooth PPy doped with KPFOS, and (3) electrochemical deposition of textured PPy doped with KPFOS. SEM micrographs of the polymer at each step of the process are shown in Figure 4-5. An electroless (chemical) deposition technique described in [62] was employed to first coat the lens paper with conductive polymer. The technique shown in Figure 4-4 involved immersing a the target substrate in a solution that contained distilled water, 0.02 M of pyrrole monomer, 0.046 M of $FeCl_3$ (the catalyst), and 0.006 M of 1,5-naphthalene disulfonic acid tetrahydrate (the initiator). The substrate was immersed for five hours at 4°C. The DC electrical impedance across the length of the resulting sample was measured to be on the order of 30 kΩ.

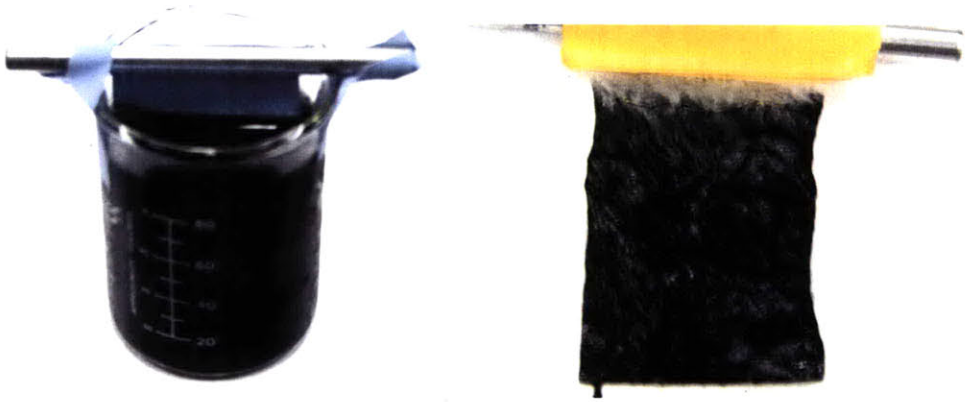

(a) Electroless deposition solution with target substrate.

(b) Lens paper substrate after electroless deposition.

Figure 4-4: The electroless deposition technique allows for the polymerization of polypyrrole on a non-conductive substrate.

A layer of smooth polypyrrole doped with KPFOS was then grown on both sides

of the sample via electrochemical deposition. The deposition solution contained acetonitrile, 0.015 M KPFOS, and 0.1 M pyrrole, and was deposited with a current density of 1.0 A/m^2, for three hours at 4°C. Gold wire was sewn around the border of the substrate to allow for better electrical contact. The resulting substrate had a DC electrical impedance of 500 Ω. The smooth PPy layer was grown on both sides of the substrate so that one side could be used as the working electrode and the other could be used as the counter electrode.

Superhydrophobic PPy was then grown electrochemically onto one side of the sample. A droplet placed on the resulting film was hydrophobic, and in the Wenzel state. The overall thickness of the film was measured to be 103 μm and the DC electrical impedance was measured to be 74 Ω. Although attempts to switch the hydrophobicity of the film were unsuccessful, this method can be used for depositing hydrophobic polypyrrole onto non-conductive substrates where it is either undesirable or impractical to deposit the substrate with a thin metallic coating.

Lens paper was coated on both sides with 60 nm of Au, and superhydrophobic PPy was grown using the procedure described in Section 2.2. PPy grew through the pores of the substrate, bridging connections between the two sides of the paper. Samples grown with this procedure were superhydrophobic with hierarchal surface roughness (Figure 4-6). Samples were able to be switched in the encapsulated device, however, because the samples were very thin, some electrolyte would seep through the pores of the polymer and reduce the hydrophobicity of the polymer. The initial state of the samples in the encapsulated device were only slightly hydrophobic with a contact angle of up to 100°. Thus, porous paper was rejected as a suitable substrate material, and mesh substrates were investigated.

4.3.3 Mesh Substrate

Mesh was explored as a more promising substrate for the working electrode because the high porosity of meshes can allow for polymer to easily grow within the pores and bridge connections between the two sides. In addition, since most mesh substrates are thicker than the porous lens paper attempted in Section 4.3.2, the issue of electrolyte

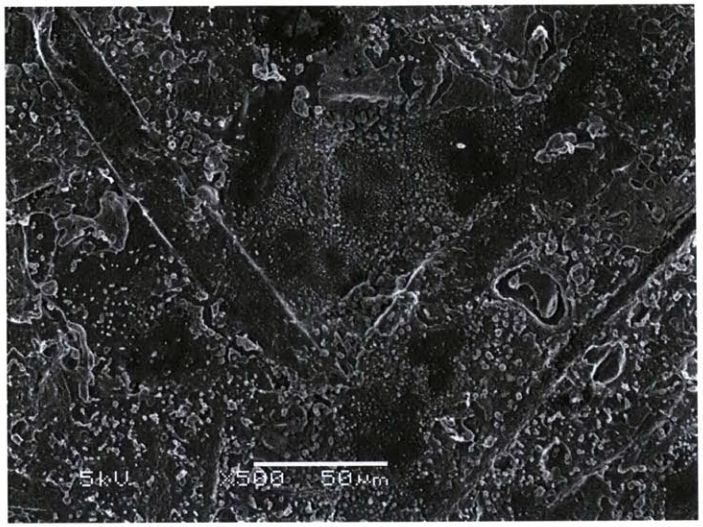

(a) Step 1: PPy grown via electroless deposition.

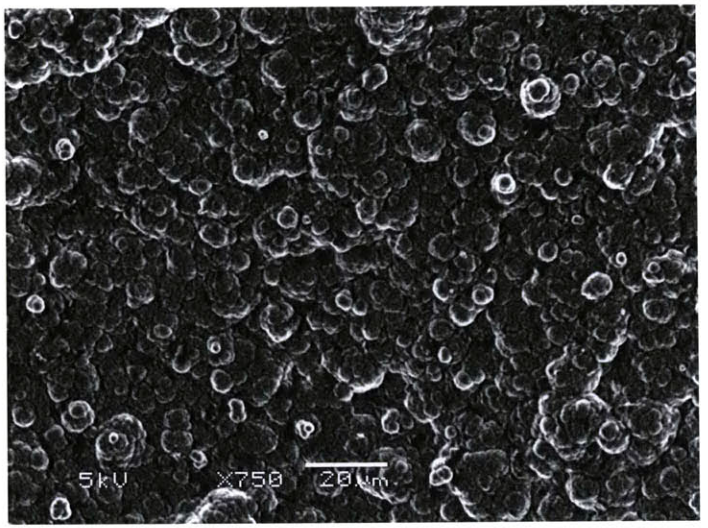

(b) Step 2: Smooth PPy grown via electrochemical deposition.

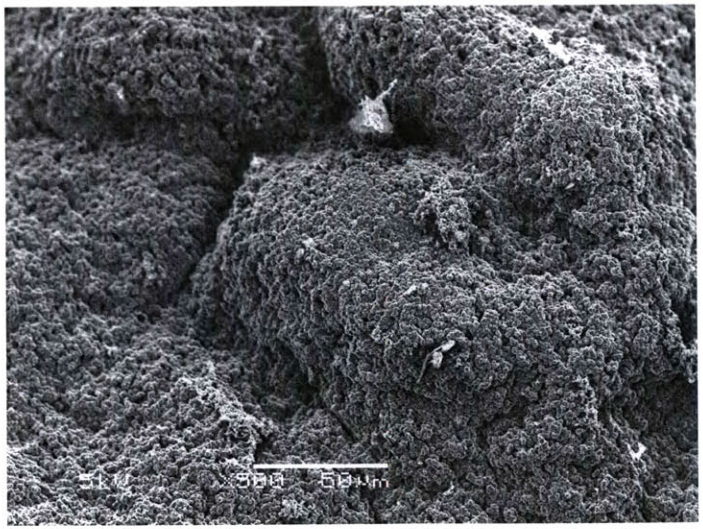

(c) Step 3: Textured PPy grown electrochemically.

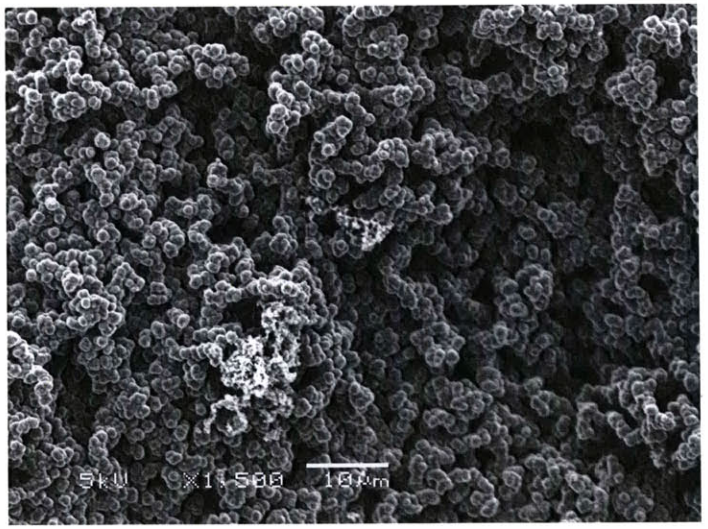

(d) Step 3: Magnified image of textured PPy.

Figure 4-5: SEM micrographs of films from metal-free deposition protocol.

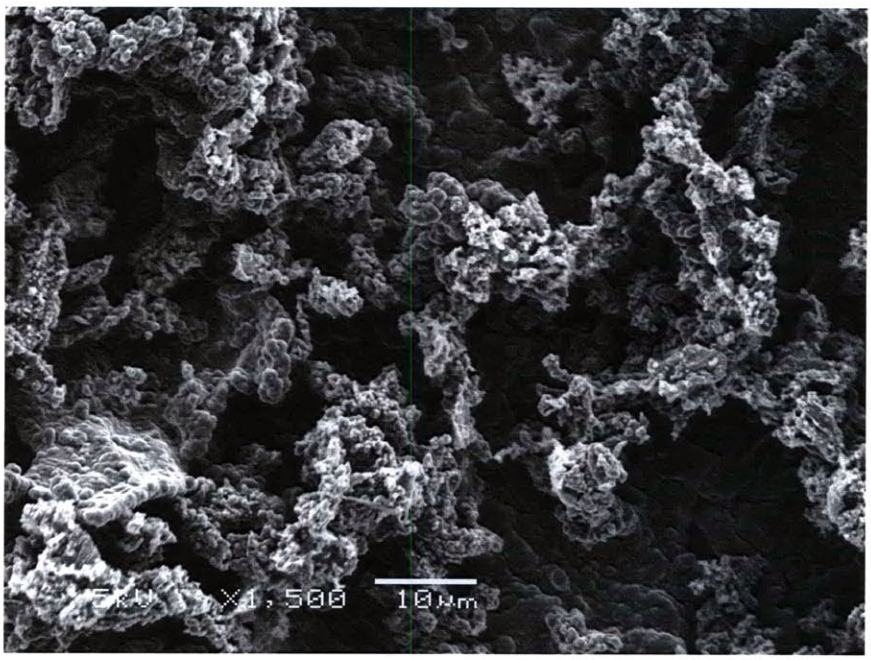

Figure 4-6: Superhydrophobic polypyrrole grown on Au-coated lens paper.

seeping through the pores of the polymer layer and mixing with the probe droplet can be more easily avoided.

Stainless Steel Mesh

Type 304 stainless steel was initially chosen as the mesh substrate due to its availability, low cost, and chemical inertness. Superhydrophobic PPy was grown onto a 180×180 stainless steel mesh with 100 μm wide square openings following the procedure described in Section 2.2. SEM micrographs shown in Figure 4-7 revealed that a thin film of smooth PPy grew over the mesh wire while the rough microstructures filled in the mesh pores. This allowed for $PFOS^-$ to travel from the surface to the electrolyte layer through the bulk of the polymer. The hydrophobicity of the PPy was greatly increased as the sample was superhydrophobic with a contact angle of up to 155°. However, the stiffness of the stainless steel prevented the polymer from making complete contact with the electrolyte layer —any kinks in the stainless steel substrate prevented the polymer from lying flat on top of the electrolyte in the encapsulated device. Stainless steel was therefore rejected as a substrate material.

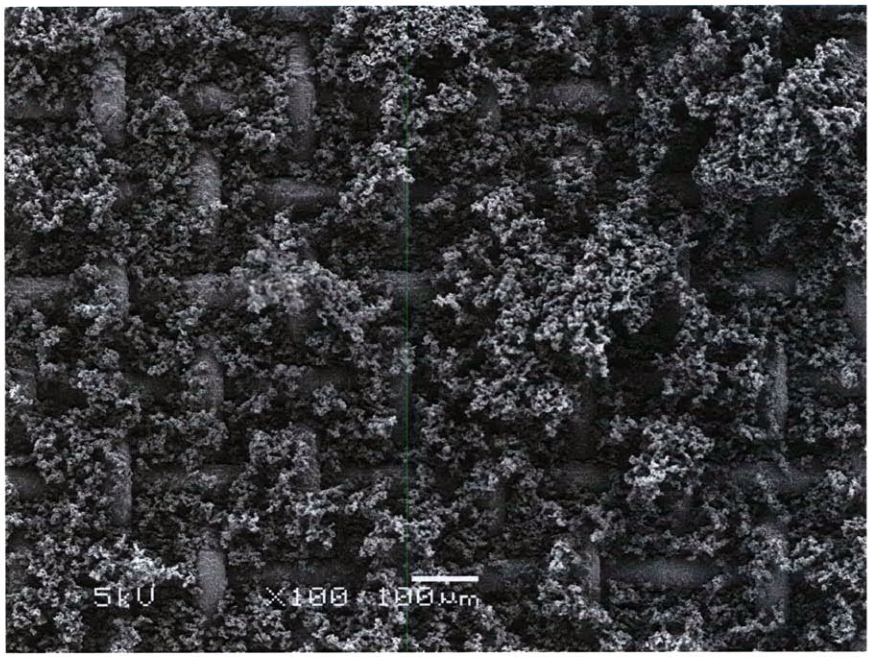

Figure 4-7: Superhydrophobic polypyrrole grown on a stainless steel mesh substrate.

Nylon Mesh

A nylon mesh substrate was chosen to allow for the PPy layer to be flexible enough to easily conform to different shapes and topographies. Thus, the area of contact between the polymer and the electrolyte is increased since the nylon substrate does not kink or bend and the polymer can conform to an electrolyte layer that is not perfectly flat.

A 168×168 precision woven nylon mesh with 90 µm wide square openings was used as the substrate. The sample was cleaned with detergent and water in a sonicator for 10 minutes, and was then rinsed with water and isoproponol. An AJA International Orion 5 Sputter Coater was used to plasma treat the substrate with an argon and oxygen mixture for one minute and then sputter coat one side of the sample with 200 nm of Au. The electrical resistance across the length of the sample was measured to be on the order of 300 Ω. Although only one side of the sample was coated with Au, both sides of the sample were found to be conductive because the conformal nature of sputter coating allows for sidewall coverage. The top side of the substrate (the side exposed to the sputtered atoms) had slightly better Au coverage and was slightly

more conductive than the bottom side (see Figure 4-8).

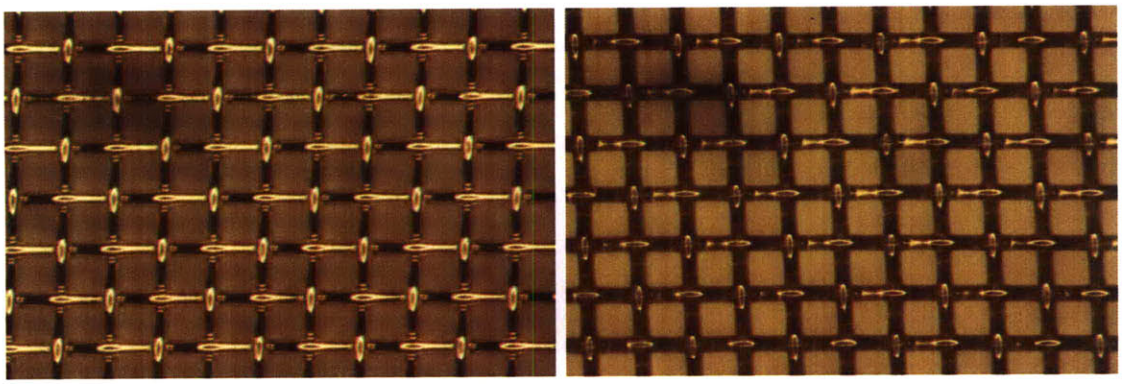

(a) Top side (b) Bottom side

Figure 4-8: Nylon mesh substrate sputter coated with 200 nm of Au.

PPy was deposited onto the nylon mesh substrate with the standard recipe described in Section 2.2. The film was superhydrophobic with a contact angle of up to 156° and a roll-off angle less than 10°. Similar to the stainless steel substrate, SEM micrographs shown in Figure 4-9 showed that a thin film of smooth PPy grew over the mesh wire while the rough microstructures grew inside the mesh pores. The microstructures grew more densely on the more conductive top side than on the bottom side of the mesh, and droplets placed on the bottom side were pinned in the Wenzel state. However, this was deemed to be acceptable since the bottom side would be in contact with the electrolyte layer. The technique of growing superhydrophobic PPy grown onto an Au-coated nylon mesh was determined to be the best method for fabricating the PPy layer for the encapsulated device due to its optimal mechanical and wettability properties and the simple fabrication process.

4.4 Development of Electrolyte Layer

The electrolyte needed to provide $PFOS^-$ ion mobility as well as have sufficiently high surface tension such that it would not seep through the pores of the polymer and wet the surface. This proved to be a significant challenge, as the solvents with which PPy is stable (*i.e.* acetonitrile, propylene carbonate) have relatively low surface

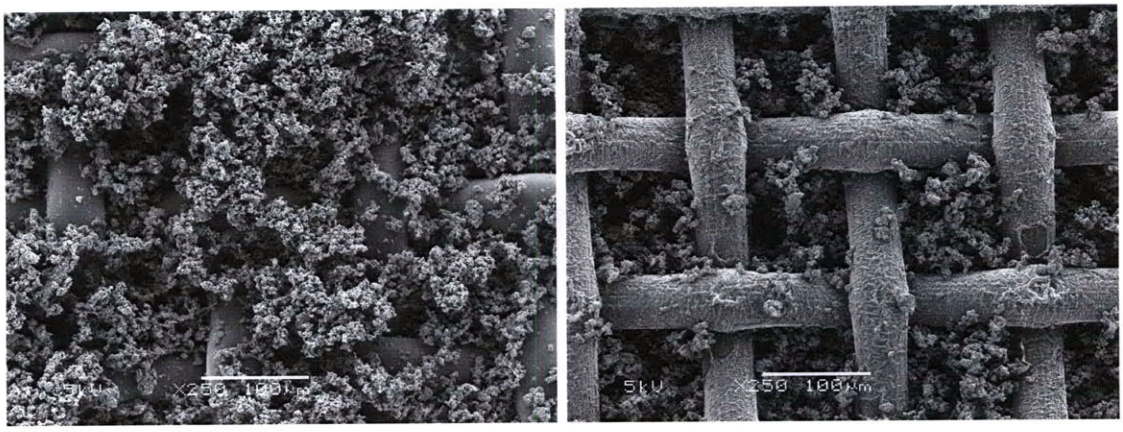

(a) Top side (b) Bottom side

Figure 4-9: Superhydrophobic polypyrrole grown on an Au-coated nylon mesh substrate.

tensions. Neat acetonitrile has a surface tension (liquid to vapor interface) of 19.1 mN/m while neat propylene carbonate has a surface tension of 41.1 mN/m. Thus, the electrolyte used in Section 2.3 (0.015 M KPFOS in acetonitrile) to switch PPy wettability in bath as well as the electrolyte used in the trilayer actuators currently in development in the BioInstrumentation Lab (propylene carbonate and salt) were unsuitable for this application.

An electrolyte modified from the gel electrolyte recipe described in [17] which was used in a previous generation of conducting polymer actuators was considered. The electrolyte described in [17] contained liquid salt (*i.e.* 1-Butyl-3-methyl-imidazolium tetrafluoroborate), a polymer that is cross-linked to form the gel (*i.e.* methacrylate), a cross-linking agent (*i.e.* dimethacrylate), and an initiator that begins the cross-linking process (*i.e.* azobisisobutyronitrile). The electrolyte was modified to contain potassium perfluorooctanesulfonate dissolved in an organic solvent instead of the liquid salt. After curing, however, the modified electrolyte had become a brittle plastic with zero ionic conductivity, and was subsequently rejected as a possible electrolyte.

An ionic liquid that contained $PFOS^-$ as the anion (*i.e.* tetrabutylammonium perfluorooctanesulfonate) was also considered for the electrolyte layer, but was ultimately rejected due to its high cost and low availability.

4.4.1 PMMA-based Gel Electrolyte

Poly(methyl methacrylate) (PMMA) based gel electrolytes belong to a class of polymeric gels that have been studied as electrolyte material for lithium ion batteries [50]. Polymeric gels are defined as systems that consist of a polymer network swollen with solvent, and possess the mechanical properties of solids but the diffusive transport properties of liquids [53]. A typical PMMA-based gel electrolyte used for lithium ion batteries contains a salt (*e.g.* $LiClO_4$, $LiAsF_6$, or $LiN(CF_3SO_2)_2$) dissolved in an organic solvent (*e.g.* propylene carbonate, ethylene carbonate, or a combination of the two) with PMMA added as a stiffener.

It has been reported that the ionic conductivity of the PMMA-based gel decreases and the viscosity of the gel increases with increasing PMMA concentration and PMMA molecular weight [9, 47]. It has also been reported that the ionic conductivity increases with increasing salt concentration [10]. The ionic conductivities of typical electrolyte solutions are dependent on the size and charge of the ion and the viscosity of the solution, and follow the relationship:

$$\mu = \frac{q}{6\pi r\eta} , \tag{4.1}$$

where μ is the carrier mobility, q is the carrier charge, r is the radius of the carrier ion, and η is the viscosity of the solution. Bohnke, *et. al* [11] observed that PMMA-based gels do not follow (4.1) as they exhibit high ionic conductivities (up to 230 mS/m at 25°C) despite having a very high macroscopic viscosity (335 Pa·s at 25 °C). They proposed that ion mobility is related to the *microscopic* viscosity rather than the macroscopic viscosity, and that ions travel through continuous paths of solvent (*i.e.* propylene carbonate) that exists within a polymer matrix. Thus, the macroscopic viscosity has little to do with the ion mobility until the PMMA concentration has surpassed a certain threshold (around 30-35 wt%) and begins to hinder ion mobility. However, Stallworth, *et. al* [52] studied the characteristics of PMMA-based gels using nuclear magnetic resonance (NMR) spectroscopy and ruled out the presence of microscopic regions of liquid electrolyte within a solid PMMA matrix, rejecting the

conclusions of Bohnke, *et. al* [11].

Although the mechanism for ion transport within PMMA-based gel electrolytes is not well understood, the electrolyte is a promising candidate for the electrolyte layer in the switching device due to its superior mechanical properties (due to its high macroscopic viscosity) and high ionic conductivity. The high flash point of propylene carbonate (132°C) allows the gel to have a very slow evaporation rate in ambient conditions.

A PMMA-based gel electrolyte was created by dissolving 0.1 M potassium perfluorooctanesulfonate in propylene carbonate. The solution was heated to 100°C and vigorously mixed as 25 wt% PMMA (100,000 molecular weight, from Alfa-Aesar) was added. The resulting gel electrolyte was extremely viscous, exhibiting almost no flow in steady-state. A TA Instruments AR-G2 stress-controlled rheometer was used to measure the gel viscosity, and the results are plotted in Figure 4-10. The gel had a low shear rate viscosity of 1000 $Pa \cdot s$, at 22°C and exhibited shear thinning at shear rates higher than 1 s^{-1}.

The ionic conductivity of the gel at ambient temperature was measured using electrochemical impedance spectroscopy (EIS). The electrochemical impedance of a system is determined by measuring the output current to an AC voltage input within a frequency range. Using the frequency response, one can then represent the system's performance by an equivalent circuit of resistors, capacitors, and inductors [5]. To measure the ionic conductivity, the gel was placed in a conductivity cell that contained two glassy carbon electrodes. The complex impedance response in the frequency range 100 Hz to 200 kHz was measured by applying a 10 mV peak to peak oscillation about 0 V at 100 points per decade, averaging five measures per frequency. The glassy carbon electrodes were assumed to be chemically inert (*i.e.* no reactions at the electrode interface) and the cell impedance was therefore dominated by the solution resistance, R_s. This assumption was confirmed by the impedance bode plot. The electrolyte had a high impedance at low frequencies, indicating that the system is dominated by mass transport at frequencies lower than 1 kHz. At frequencies higher than 1 kHz, the system can be described as an equivalent RC (series) circuit. The equivalent

circuit was fit to the impedance data using the Levenberg-Marquardt minimization technique, and a value for R_s was determined. The conductivity was then calculated from the geometry of the conductivity cell, which had a cell constant of 4.976 m^{-1}. The electrolyte had a conductivity of 14.6 $\pm$ 0.003 mS/m.

Switching devices with the PMMA-based gel as the electrolyte layer were constructed. A potentiostat was used to apply a constant voltage of -4 V, and transition times (time from when the contact angle of the droplet begins to change to when it finishes changing) varied from 1 s to 3 s. A full range of contact angles (from superhydrophobic to superhydrophilic) was achieved (Figure 4-11). There was no switch observed for applied voltages lower than -2 V.

Although PMMA-based electrolyte gels are typically used as cation conductors (*i.e.* Li^+), it is being used as an anion conductor in the switching device to transport $PFOS^-$ ions. It has been reported that the transference number of lithium ions in PMMA-based gels is between 0.4 and 0.6 [50], indicating that the transport of anions and ion pairs is occurring. This is desirable in the switching device, since the movement of $PFOS^-$ is required. The transport of the cation, K^+, is tolerable as long as cation transport does not result in a significant change in the surface energy or surface morphology.

The contact angles measured as a function of time are plotted in Figure 4-12. It can be seen that most of the wettability change occurs within the first second. It should also be noted that evaporation of fluid from the droplet due to increased surface area may have contributed in part to the change in contact angle during the last two seconds. The contact angles at both the right and left sides of the droplet were measured. In this particular case, the droplet moved slightly to the right. Thus, the contact angles on the right would be advancing contact angles while contact angles on the left were receding contact angles, which accounts for the discrepancy between the two sides.

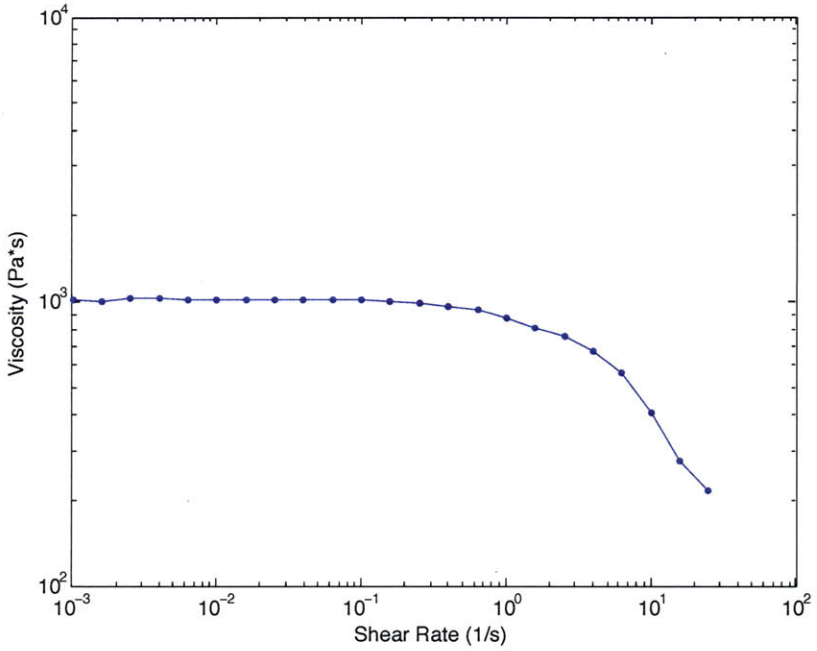

Figure 4-10: Viscosity as a function of shear rate of PMMA-based gel electrolyte.

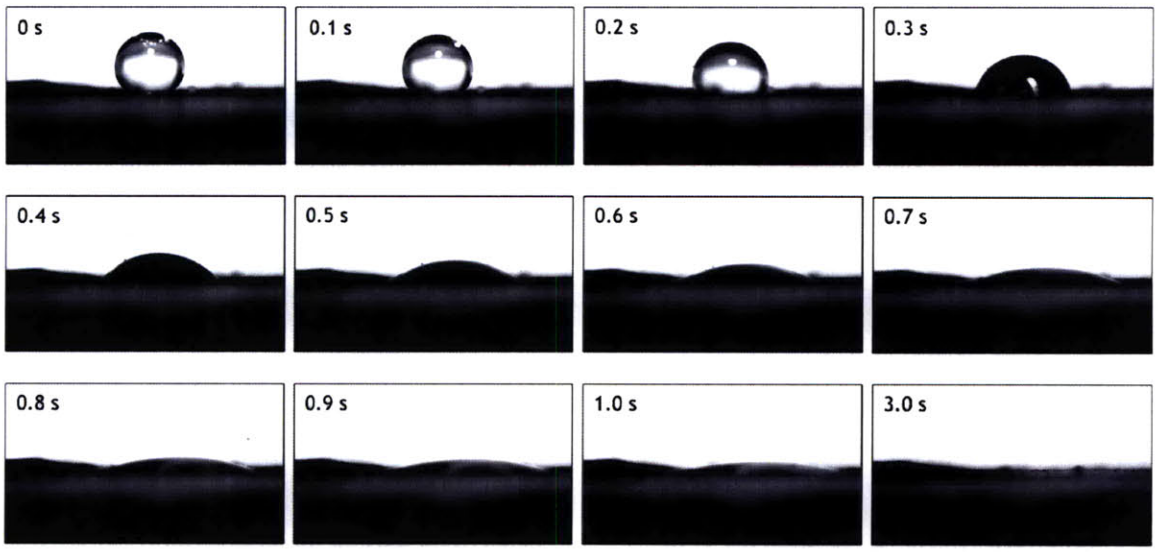

Figure 4-11: Wettability switch using the PMMA-based gel electrolyte (-4 V applied).

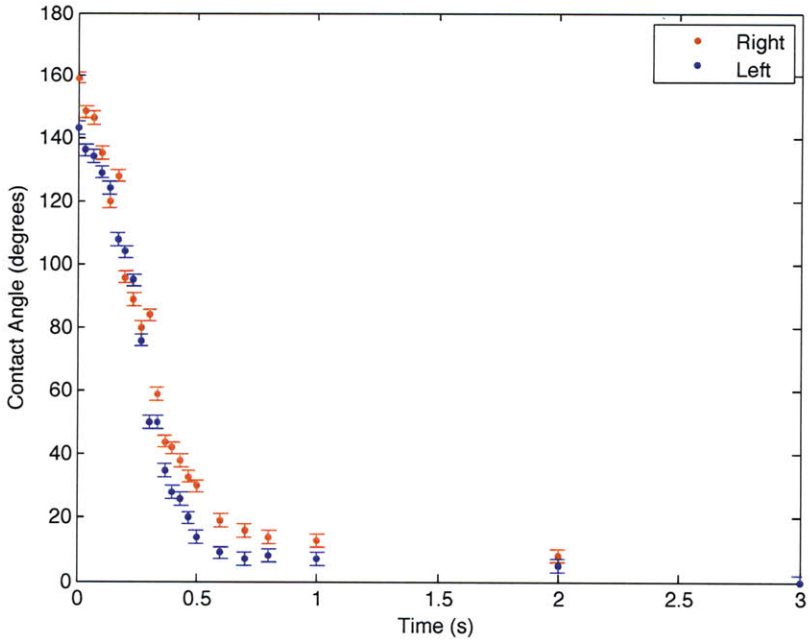

Figure 4-12: Contact angles as a function of time of an *in situ* wettability switch using the PMMA-based gel electrolyte.

4.4.2 Cellulose-based Gel Electrolyte

A cellulose-based gel electrolyte was also explored. 0.03 M of KPFOS was dissolved in an off-the-shelf hydroxyethylcellulose-based gel (Johnson and Johnson, Inc.) and used in the electrolyte layer of the switching device. The gel had a low shear rate viscosity of 150 Pa · s at 22°C and exhibited shear thinning at shear rates higher than 0.02 s^{-1} (Figure 4-13). The conductivity of the gel was 132.5 ± 0.4 mS/m.

The gel outgassed and degraded at applied voltages of -4 V and higher. Switching devices fabricated with the cellulose-based gel electrolyte exhibited much slower transition times and high variability (30 s to 90 s for an applied voltage of -3 V) when compared to the switching devices fabricated with the PMMA-based gel electrolyte. Although the cellulose-based gel electrolyte had a higher conductivity than the PMMA-based gel electrolyte, the high conductivity was due to the presence of sodium hydroxide (NaOH) in the cellulose gel. Thus, the movement of K^+, $PFOS^-$, Na^+, and OH^- ions all contributed to the gel's conductivity, and the mobility of PFOS ions in this gel was much lower than indicated by the conductivity value. Ad-

ditionally, the large variation in transition times was due to the evaporation of the water in the cellulose-based gel — the gel evaporated in 10 minutes at ambient conditions. The evaporation led to an increase in viscosity and therefore a decrease in ion mobility, according to the relationship in (4.1). Furthermore, the switching device did not exhibit the full range of contact angles — the lowest contact angle achieved was 35° as opposed to 0° with the PMMA-based gel. However, the gradual transition time makes the cellulose-based gel a promising material for applications requiring the achievement of intermediate wetting states.

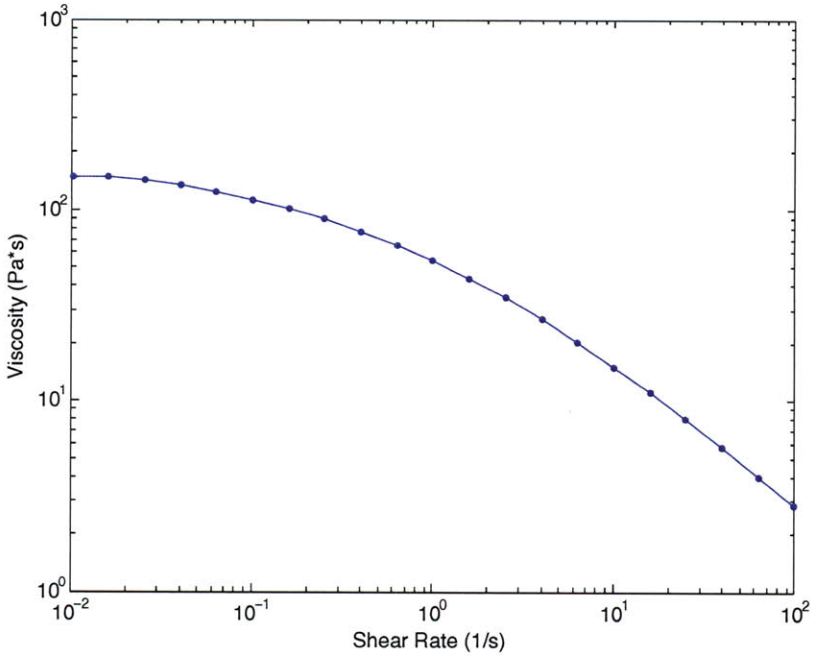

Figure 4-13: Viscosity as a function of shear rate of cellulose-based gel electrolyte.

4.4.3 Aqueous Electrolyte

An aqueous electrolyte was also used in the switching device to switch the wettability of PPy. The electrolyte contained 0.015 M KPFOS in deionized water, and had an extremely fast switching time (23 msec) due to the electrolyte's low viscosity and high ionic conductivity. The conductivity was measured to be 45.6 ± 0.022 mS/m using EIS techniques. A porous separator soaked with the aqueous electrolyte was used as the electrolyte layer in the switching device. However, the electrolyte had a

short lifetime as it dried in a few minutes in ambient conditions. Furthermore, the low viscosity of the electrolyte made it more difficult to handle as it was difficult to ensure that the entire polymer was in complete contact with the electrolyte. This caused wettability gradients to be created across the surface of the polymer, resulting in inadvertent fluid movement towards the more hydrophilic regions (Figure 4-14).

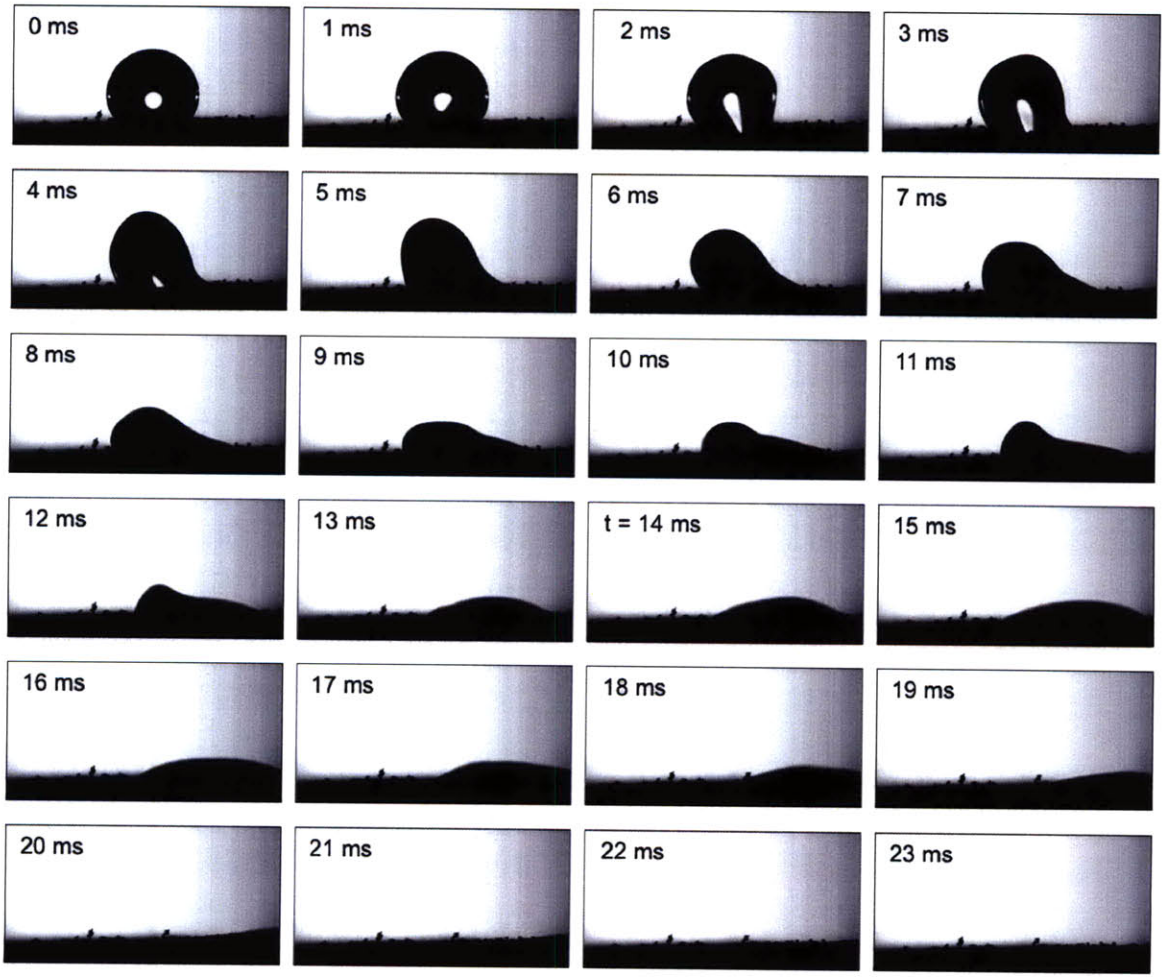

Figure 4-14: A Phantom v9 high-speed camera was used to capture the droplet behavior on the switching device at 1000 frames per second. The electrolyte contained 0.015 M KPFOS in deionized water.

4.5 Discussion

Several observations were made regarding the wettability switch using the switching device. The difference in switching times was dependent on the electrolyte used, and

can be attributed to the differences in ionic conductivities. It was also observed that the droplet tended to move towards the side where the electrode was placed (towards the right in Figure 4-2). The electrical resistance of the polymer (80 Ω in the oxidized state and 1000 Ω in the reduced state) caused a slight voltage drop across the polymer and therefore a wettability gradient.

In addition, significant droplet vibration and fluid movement inside the droplet was observed at the beginning of the switch. This can be attributed to the droplet transitioning from the initial Cassie-Baxter state to the more energetically favorable Wenzel state as the chemical composition of the surface changes. As the droplet transitions to the Wenzel state, fluid replaces the air pockets that previously existed underneath the droplet. The air bubbles displaced by fluid travel through the droplet, causing significant fluid movement inside the droplet and droplet vibration. The air bubbles can be seen through the reflection of the backlight (Figure 4-15) and were measured to be approximately 10 μm in diameter, the approximate size of the pores of PPy.

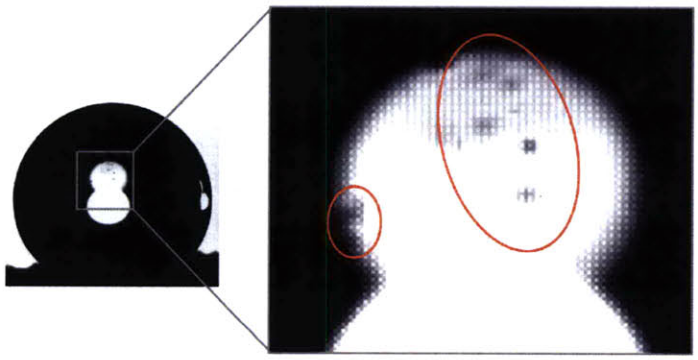

Figure 4-15: Air bubbles can be seen rising through the droplet as the droplet transitions from the Cassie-Baxter to Wenzel state.

Finally, a time delay from the onset of the applied voltage to the start of the contact angle transition was observed. The time delay was unrelated to the transition time, and was independent of the type of electrolyte. The time delay varied greatly across samples, ranging from 2 s to 138 s. There are a number of sources that could have contributed to the time delay. First, this delay may occur due to the threshold of charge that needs to be reached before the contact angle begins switching. The

time delay can be reduced by pre-treating the film with a reduction step such that the threshold is reduced. The time delay can also be caused in part by the diffusion of ions through the bulk polymer. When the polymer was switched in an electrochemical cell, the $PFOS^-$ ions just needed to come off the surface. However, in the switching device, ions need to travel through the thickness of the polymer. Furthermore, since the bulk of the material is the network of rough microstructures, the effective diffusion length is much longer than the thickness of the film since the ions need to travel long convoluted paths to leave the surface of the polymer. Variability in thicknesses across samples may have contributed to the variability in time delay. Finally, the time delay can, in part, be attributed to the contact area between the PPy layer and the electrolyte. The rough surface may have only allowed part of the surface to be in contact with the electrolyte, reducing the area of the double layer capacitance. Reducing the thickness of the film and reducing the surface roughness on the side of the polymer that contacts the electrolyte may decrease the time delay.

Chapter 5

Potential Applications and Future Work

5.1 Induced Fluid Movement

In Chapter 4, fluid movement was inadvertently induced either by a voltage gradient or by discontinuous contact between the electrolyte layer and the PPy layer. A wettability gradient can be intentionally created by modifying the electrolyte layer such that only certain areas of the polymer are in contact with the electrolyte. When a voltage is applied, ion transport occurs in the areas of polymer that are in contact with electrolyte, causing these regions to switch wettability (Figure 5-1).

A proof-of-concept device was created by modifying the electrolyte layer such that half (right side) of the polymer was in contact with the PMMA-based electrolyte described in Section 4.4.1. When a voltage was applied, the right half of the polymer was switched to a hydrophilic state, and a 3 μL droplet placed on the polymer moved towards the newly switched hydrophilic region (Figure 5-2). The center of mass of the droplet traveled approximately 2 mm in 0.8 s.

A future embodiment of such a device can utilize mesh to isolate regions containing electrolyte. Polymer regions may need to be electrically isolated to allow for the independent wettability switch of adjacent regions.

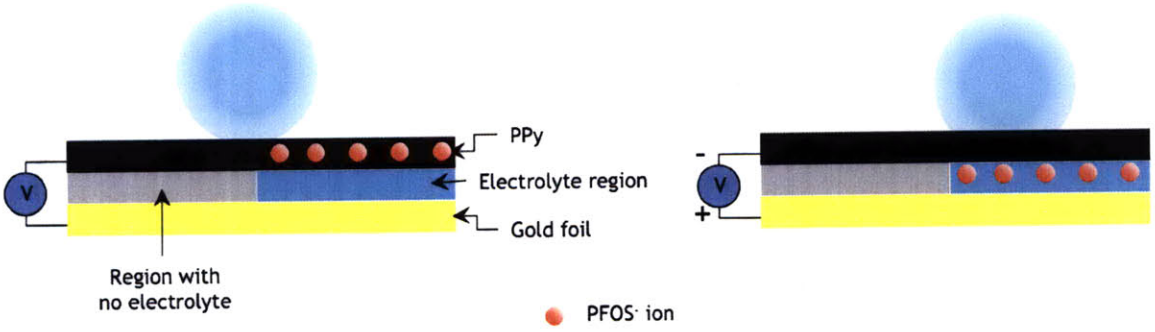

Figure 5-1: Schematic of proof-of-concept device for induced fluid movement.

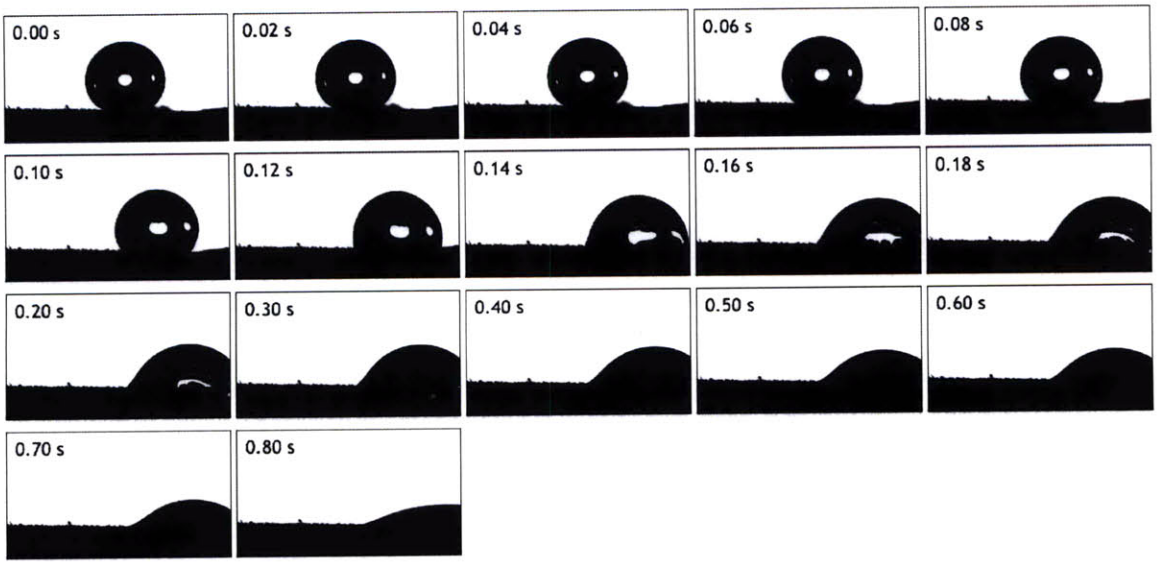

Figure 5-2: Induced fluid movement using the PPy switching device.

5.2 Oil and Water Separation

Materials that are both superhydrophobic and superoleophilic can be used for applicaitons in oil and water separation. Feng, *et. al* [23] reported coating a mesh film with a superhydrophobic and superoleophilic spray containing polytetrafluoroethylene (PTFE) which allowed for the passage of diesel oil while preventing the permeation of water (Figure 5-3).

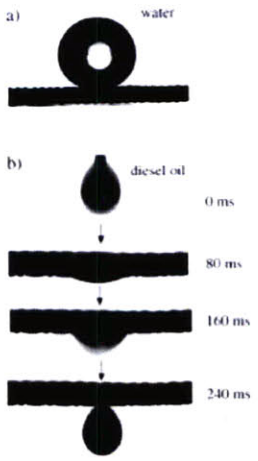

Figure 5-3: The mesh substrate coated with PTFE prevents the permeation of (a) water but allows for the passage of (b) diesel oil. From [23].

Superhydrophobic PPy was grown onto a 180×180 stainless steel mesh with 100 μm wide square openings following the procedure described in Section 2.2, except the deposition was only 30 minutes. PPy grew on the mesh wires and the PPy microstructures grew partially into the mesh pores (Figure 5-4). An emulsion of water (dyed blue) and mineral oil (clear) was dropped onto the PPy-coated mesh using a syringe. The PPy-coated mesh separated the oil from water, as the mineral oil soaked into the mesh while the water remained on top of the mesh. While the oil did not permeate through the mesh as in [23], it is believed that a mesh with larger pore size may allow for the permeation of oil. In addition, since the PPy can also be switched to a hydrophilic state, a potential application includes the 'smart' filtering of oil from water, allowing for the selective passage of water. This remains an area that requires for future development.

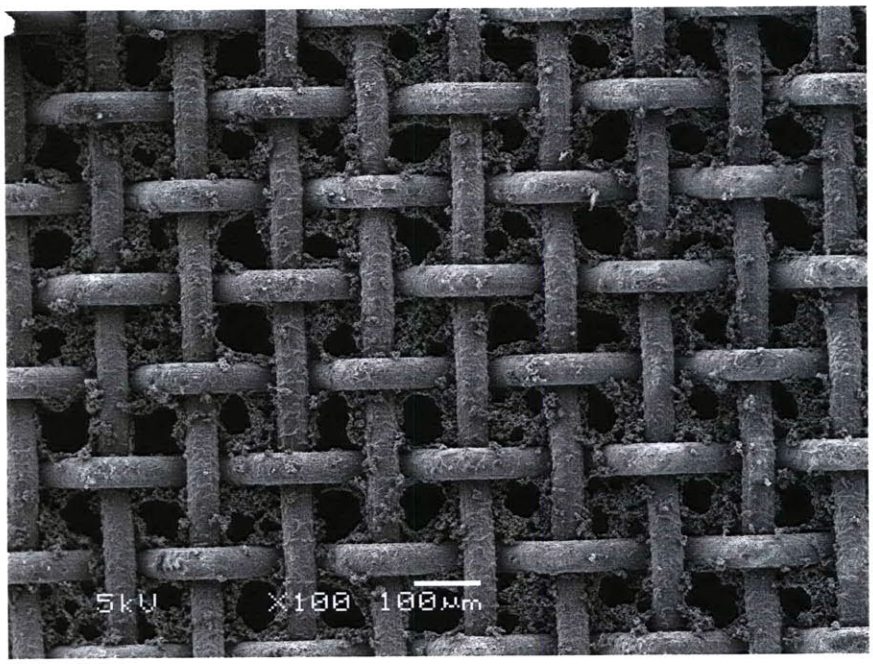

Figure 5-4: Superhydrophobic PPy grown on a stainless steel mesh for 30 minutes.

5.3 Suggestions for Future Work

5.3.1 Device Characterization

Aging

PPy is expected to undergo structural changes during the course of its lifetime that may either enhance or reduce desired conductivity and electrochemical properties [46, 48, 49]. It is also expected from previous accelerated aging studies that the effects are largely dependent on the dopant and synthesis conditions [15, 16]. However, to date there have been no studies that investigate the long-term aging effects on the electrochemical stability of PPy doped with $PFOS^-$. For this polymer to be incorporated into a useful device, the polymer's lifetime needs to be understood.

Time Delay

Section 4.5 discussed the possible sources for the time delay from the onset of the applied voltage to the beginning of the contact angle transition in the switching device. Before the switching device can be utilized in an application, the time delay needs to

be characterized and understood so that it can be reduced and possibly eliminated. If the time delay is unable to be eliminated than a model that predicts the length of the delay should be developed so that the droplet behavior can be predicted.

PMMA-based Gel Electrolyte Optimization

It has been reported that the molecular weight of PMMA, temperature of operation, salt concentration, and PMMA concentration all have an effect on the ionic conductivity and macroscopic viscosity of the polymer [9, 10, 47, 50]. The PMMA-based gel electrolyte recipe presented in Section 4.4.1 needs to be optimized for more consistent transition times and for the optimal mechanical and electrochemical properties.

5.3.2 Modeling

Surface roughness

Chapter 2 investigated the effects of different deposition parameters on the surface morphology and the reversible wettability of PPy. A model that relates the effect of the different deposition parameters to the superhydrophobicity of the polymer and the switching time will be useful for instances when the polymer needs to be tuned to have specific mechanical (*e.g.* thickness, elastic modulus, surface roughness) or electrochemical (*e.g.* switching time) properties.

Fluid Dynamics

An interesting fluid dynamics problem is the modeling of fluid movement on a chemically-induced wettability gradient. The motion and shapes of droplets placed on wettability gradients can be predicted [12, 43, 54], which is useful for practical applications of wettability gradients. A potential area for future research is the modeling of the chemical wettability gradient created by a voltage gradient and/or discontinuous contact between the WE and the electrolyte layer, and their effects on droplet motion. Furthermore, the effect of different electrolytes on the kinetics of ion transport should be

investigated to better understand the electrochemical switch and its effect on droplet motion.

5.3.3 Induced Fluid Movement

The proof-of-concept device presented in Section 5.1 can be used for directional spreading of droplets in smart cooling systems. However, for applications requiring droplet transport, intermediate wetting states need to be achieved for the implementation of fluid motion across a PPy surface. In addition, an *in situ* Wenzel to Cassie-Baxter state transition is desirable for applications requiring the minimal loss of fluid during transport or the unpinning of droplets. This thesis presented an *in situ* Cassie-Baxter to Wenzel state transition as the film was switched from superhydrophobic to superhydrophilic. When the film was oxidized in the switching device, the droplet remained pinned due to the high capillary forces acting on the droplet. A new droplet placed on the oxidized film was once again in the Cassie-Baxter state.

To create a Wenzel to Cassie-Baxter state transition, air bubbles must be introduced between the droplet and the substrate. Krupenkin, *et. al* [35] was able to introduce air bubbles the solid-liquid interface by joule heating of the substrate surface. Unfortunately, joule heating is not feasible with PPy substrates because the high current pulse required to quickly form a thin layer of vapor will irreversibly degrade the polymer. A different method for introducing air, possibly by mechanical or chemical means, needs to be explored. The unpinning of droplets remains a formidable task for researchers in this field.

Chapter 6

Summary

The chemical composition of polypyrrole can be altered by an electrical stimulus, resulting in a change in surface energy and therefore a change in the wetting state. A significant limitation of the wettability switch of PPy that has previously existed was the requirement for immersion in electrolyte to perform the switch. This thesis has laid the groundwork for PPy to be used as a material with tunable wettability.

A deposition protocol for synthesized robust microstructured PPy films was developed. The films were able to quickly and reversibly switch between the superhydrophobic and superhydrophilic states. Experiments investigating the effects of changing different deposition parameters were also presented.

A post-deposition baking treatment that decreased the charge density threshold of the PPy films was also presented. Experiments showed that the optimal treatment temperature for improved electrochemical characteristics was 150°C. Films treated at temperatures above 150°C showed significant degradation.

A switching device that allowed for the *in situ* wettability switch without immersion in electrolyte was developed. The design of the switching device required the development of a fabrication protocol for synthesizing microstructured PPy on a porous substrate. Several electrolytes that allowed for the transport of $PFOS^-$ ions through the bulk polymer were created. A PMMA-based gel electrolyte, a cellulose-based gel electrolyte, and an aqueous-based electrolyte were developed, and their advantages and disadvantages were also presented.

A proof-of-concept device that utilized wettability gradients to induce fluid movement across a PPy surface was demonstrated, and a possible application in oil and water separation was also explored.

Appendix A

MATLAB® Script to Measure Contact Angle

The following is a MATLAB® script (for Release 2008b) that uses the Image Processing Toolbox to determine the contact angle from a photograph of a droplet. The script asks the user to assign a tangent line as well as the horizon line. This method of measuring contact angle is analagous to contact angle goniometry, and has a measurement error of $\pm 2°$.

```
clear all
close all

%Prepare photo
A=imread('IMG_2316.jpg');     %reads jpeg file
B=rgb2gray(A);                %change from color to grayscale
imshow(B);                    %shows grayscale photo
crop=ginput(2);
%click top left and bottom right corner to crop
a=crop(1,1);
b=crop(1,2);
c=crop(2,1);
```

```
d=crop(2,2);
C=B(b:d, a:c);
imshow(C);

hold on

%Define tangent line
a = input('Enter when ready');  %Press 'Enter' key after zooming in
tanpoints=ginput(2);  %Use two points to define tangent line
ytan1=tanpoints(1,2);
xtan1=tanpoints(1,1);
ytan2=tanpoints(2,2);
xtan2=tanpoints(2,1);
slopetan=(ytan2-ytan1)/(xtan2-xtan1);
btan=ytan2-slopetan*xtan2;
close all
imshow(C);
hold on
for i=1:2000
    xtan(i)=i;
    ytan(i)=[xtan(i) 1]*[slopetan; btan];
end
plot(xtan, ytan, 'r')

%Use one point to define horizon line.  Assumes that substrate is flat,
%and camera is level.  Be sure to check these when taking photo.
points=ginput(1);
y_point1=points(2);
x_point1=points(1);
slopeline=0;
```

```
bline=y_point1;

%Plot horizon line
for i=1:10000
    xline(i)=i;
    yline(i)=[xline(i) 1]*[slopeline; bline];
end
plot(xline, yline,'r')



%to get angle between lines
vect1=[1 slopeline];                %get vectors of the slopes
vect2=[1 slopetan];
%use dot product of slopes to get angle
dotproduct=dot(vect1, vect2);
length1=sqrt(sum(vect1.^2));
length2=sqrt(sum(vect2.^2));
angle=acos(dotproduct/(length1*length2))*180/pi
%Output is the angle between the horizon and the tangent line,
%in degrees.  If surface is hydrophobic, be sure to subtract output
%angle from 180 to get contact angle.
```

Bibliography

[1] E. Ando, S. Onodera, M. Iino, and O. Ito. Electric conductivity changes of polypyrrole and polythiophene films with heat-treatment. *Carbon*, 39(1):101–108, 1 2001. 3.1

[2] R. Ansari and G. G. Wallace. Effect of thermal treatment on the electrochemical properties of conducting polypyrrole polymers. *Polymer*, 35(11):2372 – 2377, 1994. 3.1

[3] W. J. Bae. Cortical recording with conducting polymer electrodes. Master's thesis, Massachusetts Institute of Technology, June 2008. 1.1

[4] C. K. Baker and J. R. Reynolds. A quartz microbalance study of the electrosynthesis of polypyrrole. *Journal of Electroanalytical Chemistry*, 251(2):307 – 322, 1988. 2.2

[5] A. J. Bard and L. R. Faulkner. *Electrochemical Methods: Fundamentals and Applications*. John Wiley & Sons, Inc., New York, 2nd edition, 2000. 4.4.1

[6] P. N. Bartlett and S. K. Ling-Chung. Conducting polymer gas sensors part ii: response of polypyrrole to methanol vapour. *Sensors and Actuators*, 19(2):141 – 150, 1989. 1.1

[7] B. Berge. Electrocapillarite et mouillage de films isolants par l'eau. *Comptes Rendus de l'Académie des Sciences*, 317:157, 1993. 1.3

[8] B. Berge and J. Peseux. Variable focal lens controlled by an external voltage: an application of electrowetting. *The European Physical Journal E: Soft Matter and Biological Physics*, 3(2):159–163, 2000. 1.3

[9] O. Bohnke, G. Frand, M. Rezrazi, C. Rousselot, and C. Truche. Fast ion transport in new lithium electrolytes gelled with PMMA. i: Influence of polymer concentration. *Solid State Ionics*, 66(1-2):97–104, 1993. 4.4.1, 5.3.1

[10] O. Bohnke, G. Frand, M. Rezrazi, C. Rousselot, and C. Truche. Fast ion transport in new lithium electrolytes gelled with PMMA. ii: Influence of lithium salt concentration. *Solid State Ionics*, 66(1-2):105–112, 1993. 4.4.1, 5.3.1

[11] O. Bohnke, C. Rousselot, P. A. Gillet, and C. Truche. Gel electrolyte for solid-state electrochromic cell. *Journal of The Electrochemical Society*, 139(7):1862–1865, 1992. 4.4.1

[12] F. Brochard. Motions of droplets on solid surfaces induced by chemical or thermal gradients. *Langmuir*, 5(2):432–438, 03 1989. 5.3.2

[13] A. B. D. Cassie and S. Baxter. Wettability of porous surfaces. *Transactions of the Faraday Society*, 40:546–551, 1944. 1.2

[14] J. Causley, S. Stitzel, S. Brady, D. Diamond, and G. Wallace. Electrochemically-induced fluid movement using polypyrrole. *Synthetic Metals*, 151(1):60–64, 2005. 4.1

[15] K. Cheah, M. Forsyth, and V. T. Truong. Ordering and stability in conducting polypyrrole. *Synthetic Metals*, 94(2):215 - 219, 1998. 3.1, 5.3.1

[16] M. M. Chehimi and E. Abdeljalil. A study of the degradation and stability of polypyrrole by inverse gas chromatography, x-ray photoelectron spectroscopy, and conductivity measurements. *Synthetic Metals*, 145(1):15 - 22, 2004. 3.1, 5.3.1

[17] A. Chen. Large displacement fast conducting polymer actuators. Master's thesis, Massachusetts Institute of Technology, 2006. 1.1, 4.4

[18] T. H. Chen, Y. J. Chuang, C. C. Chieng, and F. G. Tseng. A wettability switchable surface by microscale surface morphology change. *Journal of Micromechanics and Microengineering*, 17(3):489, 2007. 1.3

[19] S. K. Cho, H. J Moon, and C. J. Kim. Creating, transporting, cutting, and merging liquid droplets by electrowetting-based actuation for digital microfluidic circuits. *Journal of Microelectromechanical Systems*, 12:70, 2003. 1.3

[20] T. Darmanin and F. Guittard. Molecular design of conductive polymers to modulate superoleophobic properties. *Journal of the American Chemical Society*, 131(22):7928–7933, Jun 10 2009. 2.1

[21] G. de Crevoisier, P. Fabre, J. M. Corpart, and L. Leibler. Switchable tackiness and wettability of a liquid crystalline polymer. *Science (New York, N.Y.)*, 285(5431):1246–1249, Aug 20 1999. 1.3

[22] P. G. de Gennes, F. Brochard-Wyart, and D. Quere. *Capillarity and Wetting Phenomena: Drops, Bubbles, Pearls, Waves.* Springer Science+Business Media, New York, 2004. 1-2

[23] L. Feng, Z. Zhang, Z. Mai, Y. Ma, B. Liu, L. Jiang, and D. Zhu. A super-hydrophobic and super-oleophilic coating mesh film for the separation of oil and water. *Angewandte Chemie- International Edition*, 43(15):2012–2014, 2004. 5.2, 5-3, 5.2

[24] X. Feng, L. Feng, M. Jin, J. Zhai, L. Jiang, and D. Zhu. Reversible superhydrophobicity to super-hydrophilicity transition of aligned ZnO nanorod films. *Journal of the American Chemical Society*, 126(1):62–63, 12 2003. 1.3

[25] C. G. L. Furmidge. Studies at phase interfaces. i. the sliding of liquid drops on solid surfaces and a theory for spray retention. *Journal of Colloid Science*, 17(4):309 – 324, 1962. 1.2.1, 1-7

[26] L. Gao and T. J. McCarthy. The "lotus effect" explained: Two reasons why two length scales of topography are important. *Langmuir*, 22(7):2966–2967, 2006. 1.2

[27] J. A. Halldorsson, S. J. Little, D. Diamond, G. Spinks, and G. Wallace. Controlled transport of droplets using conducting polymers. *Langmuir*, 25(18):11137–11141, 2009. 4.1

[28] D. L. Huber, R. P. Manginell, M. A. Samara, B. I. Kim, and B. C. Bunker. Programmed adsorption and release of proteins in a microfluidic device. *Science*, 301(5631):352–354, 2003. 1.3

[29] J. Isaksson, N. D. Robinson, and M. Berggren. Electronic modulation of an electrochemically induced wettability gradient to control water movement on a polyaniline surface. *Thin Solid Films*, 515(4):2003–2008, 2006. 4.1

[30] J. Isaksson, C. Tengstedt, M. Fahlman, N. Robinson, and M. Berggren. A solid-state organic electronic wettability switch. *Advanced Materials*, 16(4):316–320, 2004. 4.1

[31] Y. Jiang, Z. Wang, X. Yu, F. Shi, H. Xu, X. Zhang, M. Smet, and W. Dehaen. Self-assembled monolayers of dendron thiols for electrodeposition of gold nanostructures: Toward fabrication of superhydrophobic/superhydrophilic surfaces and pH-responsive surfaces. *Langmuir*, 21(5):1986–1990, 2005. 1.3

[32] K. Jurewicz, S. Delpeux, V. Bertagna, F. Bèguin, and E. Frackowiak. Supercapacitors from nanotubes/polypyrrole composites. *Chemical Physics Letters*, 347(1-3):36 – 40, 2001. 1.1

[33] A. Kaynak and E. Hâkansson. Short-term heating tests on doped polypyrrole-coated polyester fabrics. *Synthetic Metals*, 158(8-9):350 – 354, 2008. 3.1

[34] J. H. Kim, K. T. Lau, R. Shepherd, Y. Wu, G. Wallace, and D. Diamond. Performance characteristics of a polypyrrole modified polydimethylsiloxane (PDMS) membrane based microfluidic pump. *Sensors and Actuators A: Physical*, 148(1):239 – 244, 2008. 1.1

[35] T. N. Krupenkin, J. A. Taylor, E. N. Wang, P. Kolodner, M. Hodes, and T. R. Salamon. Reversible wettingdewetting transitions on electrically tunable superhydrophobic nanostructured surfaces. *Langmuir*, 23(18):9128–9133, 2007. 5.3.3

[36] G. Lippmann. Relations entre les phénomènes électriques et capillaires. *Annales des Chimie et des Physique*, 5:494, 1875. 1.3

[37] M. Liu, F. Q. Nie, Z. Wei, Y. Song, and L. Jiang. In situ electrochemical switching of wetting state of oil droplet on conducting polymer films. *Langmuir*, 26(6):3993–3997, 2009. 4.1

[38] J. D. Madden, R. A. Cush, T. S. Kanigan, and I. W. Hunter. Fast contracting polypyrrole actuators. *Synthetic Metals*, 113(1-2):185–192, 2000. 1.1

[39] J. D. W. Madden. *Conducting polymer actuators.* PhD thesis, Massachusetts Institute of Technology, 2000. 1.3.1, 2-1

[40] P. Madden. *Development and Modeling of Conducting Polymer Actuators and the Fabrication of a Conducting Polymer Based Feedback Loop.* PhD thesis, Massachusetts Institute of Technology, August 2003. 1-9

[41] F. Mugele and J. C. Baret. Electrowetting: from basics to applications. *Journal of Physics: Condensed Matter*, 17, 2005. 1.3

[42] T. Osaka, T. Momma, H. Ito, and B. Scrosati. Performances of lithium/gel electrolyte/polypyrrole secondary batteries. *Journal of Power Sources*, 68(2):392–396, 1997. 1.1

[43] L. M. Pismen and U. Thiele. Asymptotic theory for a moving droplet driven by a wettability gradient. *Physics of Fluids*, 18, 2006. 5.3.2

[44] R. Z. Pytel. *Artificial muscle morphology: structure/property relationships in polypyrrole actuators.* PhD thesis, Massachusetts Institute of Technology, June 2007. 1-8, 2.2

[45] B. Ruddy. Conducting polymer wires for intravascular neural recording. Master's thesis, Massachusetts Institute of Technology, June 2006. 1.1

[46] S. Sakkopoulos, E. Vitoratos, and E. Dalas. Conductivity degradation due to thermal aging in conducting polyaniline and polypyrrole. *Synthetic Metals*, 92(1):63–67, 1 1998. 5.3.1

[47] J. P. Sharma and S. S. Sekhon. PMMA-based polymer gel electrolytes containing NH4PF6: role of molecular weight of polymer. *Materials Science and Engineering: B*, 129(1-3):104–108, 2006. 4.4.1, 5.3.1

[48] B. Sixou, N. Mermilliod, and J. P. Travers. Aging effects on the transport properties in conducting polymer polypyrrole. *Physical Review B*, 53(8), 02 1996. 5.3.1

[49] B. Sixou, M. Vautrin, A. J. Attias, and J. P. Travers. Conductivity evolution of polypyrrole thin films with aging. *Synthetic Metals*, 84(1-3):835–836, 1 1997. 5.3.1

[50] J. Y. Song, Y. Y. Wang, and C. C. Wan. Review of gel-type polymer electrolytes for lithium-ion batteries. *Journal of Power Sources*, 77(2):183–197, 1999. 4.4.1, 4.4.1, 5.3.1

[51] V. Srinivasan, V. K. Pamula, and R. B. Fair. An integrated digital microfluidic lab-on-a-chip for clinical diagnostics on human physiological fluids. *Lab on a Chip*, 4:310, 2004. 1.3

[52] P. E. Stallworth, S. G. Greenbaum, F. Croce, S. Slane, and M. Salomon. Lithium-7 NMR and ionic conductivity studies of gel electrolytes based on poly(methylmethacrylate). *Electrochimica Acta*, 40(13-14):2137 – 2141, 1995. International symposium on polymer electrolytes. 4.4.1

[53] R. F. Stepto, editor. *Polymer networks: Principles of their formation, structure, and properties.* Springer, 1998. 4.4.1

[54] R. S. Subramanian, N. Moumen, and J. B. McLaughlin. Motion of a drop on a solid surface due to a wettability gradient. *Langmuir*, 21(25):11844–11849, 2005. 5.3.2

[55] T. Sun, L. Feng, X. Gao, and L. Jiang. Bioinspired surfaces with special wettability. *Accounts of Chemical Research*, 38(8):644–652, 2005. 1-4

[56] T. Sun, G. Wang, L. Feng, B. Liu, Y. Ma, L. Jiang, and D. Zhu. Reversible switching between superhydrophilicity and superhydrophobicity. *Angewandte Chemie- International Edition*, 43(3):357–360, 2004. 1.3

[57] United Test JYSP-180 Contact Angle Goniometer. *United Test Co.* Web. 05 Aug. 2010. http://www.unitedtest.com/cp/html/?88.html. 1-5

[58] G. Wallace and P. Innis. Inherently conducting polymer nanostructures. *Journal of Nanoscience and Nanotechnology*, 2(5):441–451, October 2002. 1.1

[59] M. Wan. A template-free method towards conducting polymer nanostructures. *Adv.Mater*, 20:2926–2932, 2008. 2.1

[60] X. Wang, M. Berggren, and O. Inganäs. Dynamic control of surface energy and topography of microstructured conducting polymer films. *Langmuir*, 24(11):5942–5948, 2008. 2.1

[61] R. N. Wenzel. Resistance of solid surfaces to wetting by water. *Industrial & Engineering Chemistry*, 28(8):988–994, 1936. 1.2

[62] N. S. Wiedenman. *Towards programmable materials - tunable material properties through feedback control of conducting polymers.* PhD thesis, Massachusetts Institute of Technology, June 2008. 4.3.2

[63] J. Y. Wong, R. Langer, and D.E. Ingber. Electrically conducting polymers can noninvasively control the shape and growth of mammalian cells. *Proceedings of the National Academy of Sciences*, 91(8), 1994. 1.1

[64] F. Xia, Y. Zhu, and L. Jiang. Smart responsive surfaces switching reversibly between super-hydrophobicity and super-hydrophilicity. *Soft Matter*, 5:275–281, 2009. 1.3

[65] L. Xu, W. Chen, A. Mulchandani, and Y. Yan. Reversible conversion of conducting polymer films from superhydrophobic to superhydrophilic. *Angewandte Chemie- International Edition*, 44(37), 2005. 2.1, 2.2, 2.2, 2.3

[66] T. Young. An essay on the cohesion of fluids. *Philosophical Transactions of the Royal Society of London*, 95:65–87, 1805. 1.2